Bioorganic Chemistry 119 (2022) 105516

Contents lists available at ScienceDirect

Bioorganic Chemistry

journal homepage: www.elsevier.com/locate/bioorg

Cyclometalated Ru(II)-isoquinoline complexes overcome cisplatin resistance of A549/DDP cells by downregulation of Nrf2 via Akt/GSK-3β/Fyn pathway

Lanmei Chen [a,b,1], Jie Wang [a,1], Xianhong Cai [a], Suxiang Chen [c], Jingjing Zhang [d,e], Baojun Li [a], Weigang Chen [a], Xinhua Guo [a], Hui Luo [a,b,e,*], Jincan Chen [a,b,e,*]

[a] Guangdong Key Laboratory for Research and Development of Natural Drugs, The Marine Biomedical Research Institute, School of Pharmacy, Guangdong Medical University, Zhanjiang 524023, China
[b] Southern Marine Science and Engineering Guangdong Laboratory (Zhanjiang), Zhanjiang, Guangdong 524023, China
[c] Centre for Molecular Medicine and Innovative Therapeutics, Murdoch University, Perth, Western Australia 6150, Australia
[d] Affiliated Hospital of Guangdong Medical University & Key Laboratory of Zebrafish Model for Development and Disease of Guangdong Medical University, Zhanjiang 524001, China
[e] The Marine Biomedical Research Institute of Guangdong Zhanjiang, Zhanjiang, Guangdong 524023, China

ARTICLE INFO

Keywords:
Cyclometalated Ru(II)-isoquinoline complexes
Nrf2
Cisplatin resistance
Akt/GSK-3β/Fyn

ABSTRACT

Both ruthenium (Ru) and isoquinoline (IQ) compounds are regarded as potential anticancer drug candidates. Here, we report the synthesis and characterization of three novel cyclometalated Ru(II)-isoquinoline complexes: **RuIQ-3**, **RuIQ-4**, and **RuIQ-5,** and evaluation of their *in vitro* cytotoxicities against a panel of cell lines including A549/DDP, a cisplatin-resistant human lung cancer cell line. A549/DDP 3D multicellular tumor spheroids (MCTSs) were also used to detect the drug resistance reversal effect of Ru(II)-IQ complexes. Our results indicated that the cytotoxic activities against cancer cells of Ru(II)-IQ complexes, especially **RuIQ-5**, were superior compared with cisplatin. In addition, **RuIQ-5** exhibited low toxicity towards both normal HBE cells *in vitro* and zebrafish embryos *in vivo*. Further investigation on cellular mechanism of action indicated that after absorption by A549/DDP cells, **RuIQ-5** was mainly distributed in the nucleus, which is different from cisplatin. Besides, **RuIQ-5** could induce apoptosis through mitochondrial dysfunction, reactive oxygen species (ROS) accumulation, ROS-mediated DNA damage, and cycle arrest at both S and G2/M phases. Moreover, **RuIQ-5** could inhibit the overexpression of Nrf2 through regulation of Akt/GSK-3β/Fyn signaling pathway and hindering the nuclear translocation of Nrf2. Based on these findings, we firmly believe that the studied Ru(II)-IQ complexes hold great promise as anticancer therapeutics with high effectiveness and low toxicity.

1. Introduction

Lung cancer is the most frequent cause of cancer-related deaths worldwide. Non-small cell lung cancer (NSCLC) is a highly metastatic and aggressive subtype, accounting for about 80% of all lung cancer cases [1]. Chemotherapy is an important part of comprehensive treatment for lung cancer patients. Cisplatin (DDP) is one of the common chemotherapeutic agents for the treatment of NSCLC, however, the efficacy and the spectrum of anti-tumor activities of cisplatin is significantly compromised due to drug resistance and induced side effects. Therefore, the clinical application of cisplatin has been greatly limited [2,3]. Cisplatin resistance in lung cancer is closely associated with aberrant activation of the nuclear factor erythroid 2-related factor 2 (Nrf2) [4].

Nrf2 is a nuclear factor that coordinates the expression and induction of a battery of cytoprotective proteins-encoding genes [5]. Under normal conditions, Nrf2 acts as a transcription factor that plays a key role in the regulation of normal cells in generating protective responses and resisting adverse effects of external stress stimuli. However, upon stimulation by internal and external free radicals or chemicals, Nrf2 is

* Corresponding authors at: Guangdong Key Laboratory for Research and Development of Natural Drugs, The Marine Biomedical Research Institute, School of Pharmacy, Guangdong Medical University, Zhanjiang 524023, China.
E-mail addresses: luohui@gdmu.edu.cn (H. Luo), jincanchen@126.com (J. Chen).
[1] L. Chen and J. Wang contribute equally to this work.

https://doi.org/10.1016/j.bioorg.2021.105516
Received 7 June 2021; Received in revised form 18 November 2021; Accepted 21 November 2021
Available online 25 November 2021

overexpressed, leading to enhanced expression of protective genes including those encoding phase II detoxification enzymes, antioxidant enzymes, and multidrug resistance protein (MRP) in response to stimuli, and thus promoting tumor drug resistance [6,7]. Therefore, Nrf2 has become an attractive therapeutic target for cisplatin resistance. Recent studies revealed that the function of Nrf2 can be regulated by the Akt/GSK-3β/Fyn pathway via controlling Fyn-mediated export and degradation of nuclear Nrf2 [8–10]. Inhibition of the Nrf2 signaling pathway can reverse the drug resistance of lung cancer cells, thus enhancing the efficacy of chemotherapy [11–14]. Recent studies also demonstrated that inhibition of the Nrf2 pathway could block drug resistance in both NSCLC cells and mice bearing NSCLC xenografts [15,16].

Isoquinoline (IQ) and its derivatives are among the alkaloids with nitrogen heterocyclic structure which exist widely in nature and possess a variety of physiological activities, such as anticancer, analgesic, and anti-inflammatory [17]. In terms of anticancer activity, isoquinoline alkaloids can inhibit the proliferation, migration and invasion of tumor by many ways, such as cell cycle arrest, induction of apoptosis, and inhibition of the activities of cyclooxygenase-2 (COX-2), telomerase, and topoisomerase [18]. In recent years, many studies have shown that isoquinoline alkaloids can reverse multidrug resistance (MDR) of tumor cells. For instance, Li et al. reported that isoquinoline derivative **HZ08** can block Adriamycin (ADM) resistance of MCF-7/ADM cells through inhibition of drug efflux protein, P-glycoprotein (P-gp) [19,20]. Lei et al. reported that isoquinoline alkaloids extracted from *Rhizoma Corydalis* can inhibit the transcription of multidrug resistance gene 1 (*MDR1*) and multidrug resistance associated protein 1 (*MRP1*), and thus reduce the production of P-gp (coded by *MDR1*) and MRP1 (coded by *MRP1*), leading to reversal of the drug resistance of MCF-7/ADR [21]. Zeng et al. summarized twenty-six types of isoquinoline alkaloids and found that some of the alkaloids displayed more potent anti-MDR effects than the positive control, against the tested cancer cells [22]. In addition, Liang et al. showed that the antitumor activities of the metal (Zn^{2+}, Ni^{2+}, Cu^{2+})-isoquinoline derivatives coordination complexes are significantly higher than that of the isoquinoline ligands alone, indicating that isoquinoline derivatives are ideal metal ligands [23].

Ruthenium (Ru) complexes have attracted a great deal of interest as anticancer drug candidates because of their low toxicity, diverse mechanisms of action, and non-cross resistance in contrast to the conventional platinum (Pt)-based agents. In recent decades, an increasing number of reports have supported that Ru complexes have emerged as the most outstanding candidates for cancer treatment [24]. Ru compounds have shown selective bioactivity and the capability of overcoming the resistance that Pt-based therapeutics face, making them competitive oncotherapeutic candidates in rational drug design approaches [25]. So far, four Ru complexes including imidazolium(imidazole)-(dimethylsulfoxide) tetrachlororuthenate(III) (**NAMI-A**) [26,27], indazolium *trans*-tetrachlorobis(1*H*-indazole) ruthenium(III)] (**KP1019**) [28,29], **KP133929** [30] and Ru(II)-based therapeutics **TLD1433** [31] have entered clinical trials. In addition, Ru(II) compound **DW1/2**, a protein kinase inhibitor, is currently in preclinical development stage [25,32]. Chao et al. found that tridentate ring cyclometalated Ru complex $[Ru(pbpy)(adtpy)]^+$ exhibits effective inhibitory activity against A549 human NSCLC cells and cisplatin resistant A549/DDP cells with half-maximal inhibitory concentration (IC_{50}) values of 0.55 μM and 0.57 μM, respectively [33]. Another cyclometalated Ru complex, $[Ru(phen)(bzq)(tbtfpip)]^+$ has displayed 178-fold higher anti-tumor activity against A549/DDP cells than cisplatin. Further studies showed that there was no significant difference in absorption rates of $[Ru(phen)(bzq)(tbtfpip)]^+$ between A549 and A549/DDP cells [34]. After absorption by cells, this complex was mainly concentrated in mitochondria and could downregulate the expression level of thioredoxin reductase (TrxR). This distinct mechanism of action might be the main reason for the reversal of A549/DDP resistance [34,35].

Encouraged by these findings, we synthesized three novel Ru(II) complexes with isoquinoline (IQ) as main ligand: $[Ru(bpy)_2(1\text{-}(4\text{-F-Ph})\text{-IQ})]^+$ (bpy = 2,2′-bipyridine, **RuIQ-3**), $[Ru(bpy)_2(1\text{-}(4\text{-F-Ph})\text{-}7\text{-}OCH_3\text{-IQ})]^+$ (**RuIQ-4**) and $[Ru(bpy)_2(1\text{-}(4\text{-F-Ph})\text{-}6,7\text{-}(OCH_3)_2\text{-IQ})]^+$ (**RuIQ-5**) (see Fig. 1), and evaluated their anticancer activity on different human carcinoma cell lines. **RuIQ-5** was then identified as the best performing complex among them. Further examination of IC_{50} value for **RuIQ3**-**RuIQ-5** in 3D multicellular tumor spheroids (MCTSs) confirmed its superior anticancer efficacy *in vitro*. It is worth mentioning that **RuIQ-5** displayed selective cytotoxicity to cancer cells that it exhibited only low toxicity on both normal HBE cells *in vitro* and zebrafish embryos *in vivo*. Subsequent investigation on the mechanism of tumor inhibition effect showed that **RuIQ-5** could induce ROS-mediated apoptosis of A549/DDP cells through Nrf2 inhibition. The study also revealed that **RuIQ-5** could trigger mitochondrial dysfunction and DNA damage, while it inhibited protein kinase B (PKB or Akt) and Glycogen synthase kinase (GSK-3β) signaling pathway. Taken together, our results indicated that Ru(II)-isoquinoline complexes tested in this work could be developed as Nrf2 inhibitors that reverse the drug resistance of A549/DDP cells, demonstrating the promise and potential of Ru(II)-isoquinoline complexes as effective and safe NSCLC therapeutics.

2. Results and discussion

2.1. Synthesis and characterization

The synthetic routes of precursor *cis*-$[Ru(bpy)_2Cl_2]$ (L = bpy, phen), ligands 1-(4-F-Ph)-IQ, 1-(4-F-Ph)-7-OCH_3-IQ, and 1-(4-F-Ph)-6,7-$(OCH_3)_2$-IQ, and the cyclometalated Ru(II)-IQ complexes **RuIQ-3**, **RuIQ-4**, and **RuIQ-5** are depicted in Scheme 1. Firstly, the ligands 1-(4-F-Ph)-IQ, 1-(4-F-Ph)-7-OCH_3-IQ, and 1-(4-F-Ph)-6,7-$(OCH_3)_2$-IQ were synthesized according to the previously reported method [36]. Secondly, the precursor *cis*-$[Ru(bpy)_2Cl_2]\cdot 2H_2O$ was obtained through reflowing $RuCl_3\cdot nH_2O$,LiCl and bpy in N,*N*-Dimethylformamide (DMF) solution at 140 °C overnight [37,38]. Finally, complexes **RuIQ-3**, **RuIQ-4**, and **RuIQ-5** were obtained by reacting *cis*-$[Ru(bpy)_2Cl_2]$ with 1-(4-F-Ph)-IQ, 1-(4-F-Ph)-7-OCH_3-IQ, or 1-(4-F-Ph)-6,7-$(OCH_3)_2$-IQ in ethyl alcohol at 80 °C overnight under the protection of argon. Then, complexes **RuIQ-3**, **RuIQ-4**, and **RuIQ-5** were characterized by electrospray ionization mass spectrometry (ESI-MS, Fig. S1–S3 in supplementary materials), and proton nuclear magnetic resonance (^1H NMR and ^{13}C NMR, Fig. S4–S9 in supplementary materials). The counter anion of all these complexes is PF_6^-.

2.2. Stability and UV–visible spectral studies

Stability of antineoplastic drugs is essential to ensure their efficacy and safety. The stability of the synthesized cyclometalated Ru(II)-IQ complexes in aqueous solution was tested by UV–vis spectroscopy. As shown in Fig. S10-S12 in supplementary materials, the Ru(II)-IQ complexes were basically stable in phosphate buffer saline (PBS) within 48 h that the UV absorption peak showed no obvious change. The UV–visible spectral characteristics of the complexes are similar to those of other isoquinoline Ru complexes [39]. **RuIQ-3**, **RuIQ-4**, and **RuIQ-5** showed intense absorption bands in the range of 260–300 nm, which was attributed mainly to intra-ligand π-π* transitions. The relatively weak bands at 330–400 nm were most likely attributed to π-π* transitions. The relatively broad and weak absorption bands at 425–590 nm were assigned to the metal-to-ligand charge transfer (MLCT) absorption.

2.3. Cytotoxicity on 2D cancer cell cultures

The *in vitro* cytotoxicities of Ru(II)-IQ complexes **RuIQ-3**, **RuIQ-4**, and **RuIQ-5** against four selected human cancer cell lines (lung adenocarcinoma A549, cisplatin resistant A549/DDP, hepatocellular carcinoma HepG2, and breast cancer MCF-7) and one human normal bronchial epithelial cell line HBE were determined by 3-(4,5-dimethylthiazol-2-yl)-2,5-diphenyltetrazolium bromide (MTT) assay after co-

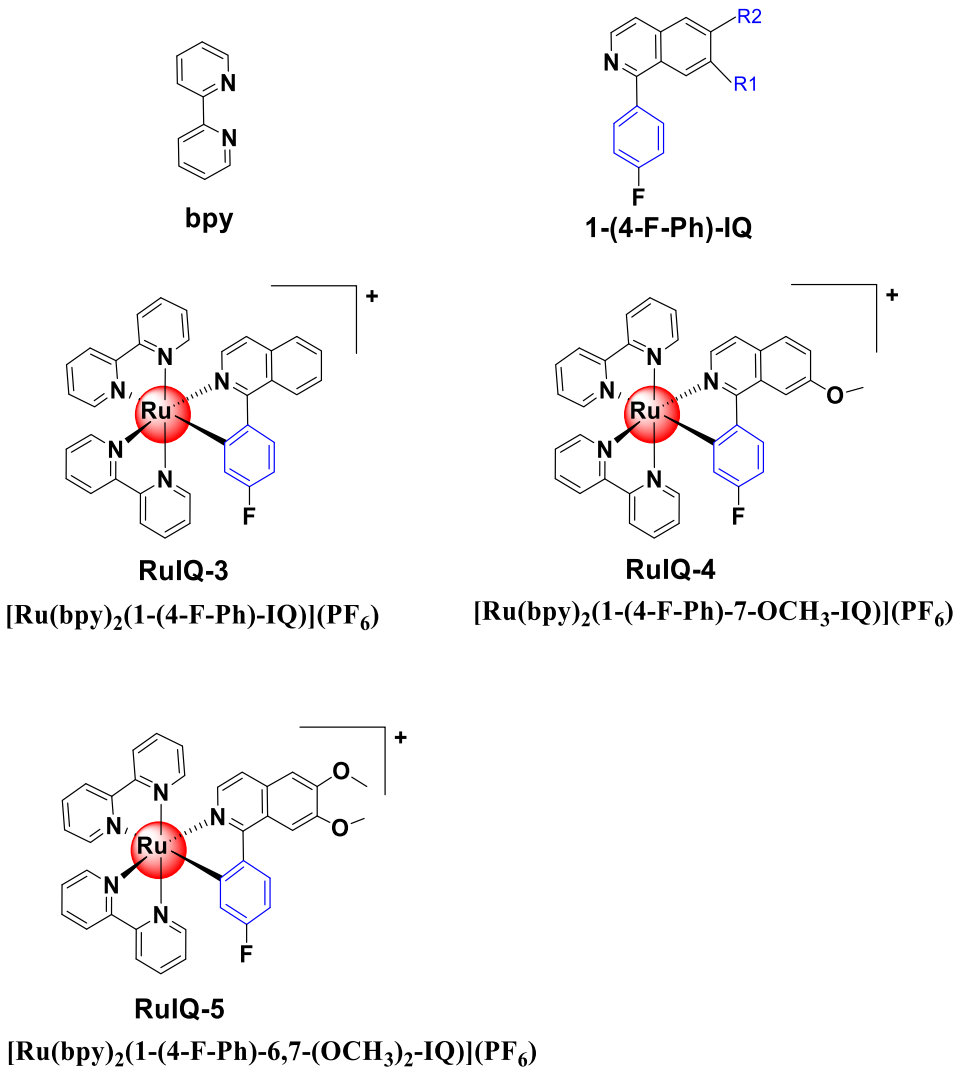

Fig. 1. The chemical structure of ligand bpy, 1-(4-F-Ph)-IQ and Ru(II) complexes **RuIQ-3**, **RuIQ-4**, and **RuIQ-5**.

incubation of cells with Ru(II)-IQ complexes for 48 h. The chemotherapeutic agent cisplatin was chosen as a positive control. As shown in Table 1, the IC_{50} values of the ligands 1-(4-F-Ph)-IQ, 1-(4-F-Ph)-7-OCH_3-IQ, 1-(4-F-Ph)-6,7-$(OCH_3)_2$-IQ and the precursor *cis*-$[Ru(bpy)_2Cl_2]$ against the tested cancer cell lines all exceeded 150 μM, and therefore, these ligands and precursor were deemed ineffective when used alone. In contrast, the cyclometalated Ru(II)-IQ complexes exhibited greatly enhanced cytotoxicities and were more potent than cisplatin against the cancer cell lines. The IC_{50} values of the Ru(II)-IQ complexes (**RuIQ-3**: 4.5 μM, **RuIQ-4**: 3.8 μM, **RuIQ-5**: 2.2 μM) against A549 cells were much lower than those of cisplatin (15.6 μM) and other structurally similar non-cyclometalated Ru(II) complexes [39]. It's worth noting that the selectivity index (SI) of the cyclometalated Ru(II)-IQ complexes (**RuIQ-3**, **RuIQ-4**, **RuIQ-5**) is about 5–8 times the SI of cisplatin. Moreover, **RuIQ-3**, **RuIQ-4**, and **RuIQ-5** showed potent inhibitory activities against cisplatin-resistant A549/DDP as well, with their resistant factor (RF) values close to 1.0, which were lower than 3.13 in the positive control (cisplatin) group. The higher SI and lower RF values of the Ru(II)-IQ complexes suggests that they possess higher efficacy and improved safety profile as potential cancer therapeutics, which was also supported by previous reports [40,41]. In order to confirm the cytotoxic effect of the Ru(II)-IQ complexes on lung cancer cells, MTT assay was performed with a concentration gradient of each complex and a time gradient for the A549 and A549/DDP cells (Fig. S13 in supplementary information). As shown in Fig. S13, treatment of Ru(II)-IQ complexes (**RuIQ-3**, **RuIQ-4**, **RuIQ-5**) resulted in marked reduction in the viability of A549 and A549/DDP cells in a concentration- and time-dependent manner. Since **RuIQ-5** was identified as the most efficacious candidate among the three Ru(II)-IQ complexes, it was thereby chosen for further investigations.

To verify the anti-proliferation ability of the complex **RuIQ-5** on A549 and A549/DDP cells, wound-healing assay was performed. As shown in Fig. 2, after treatment of cells with 2.0 μM of **RuIQ-5** for 24 h, the wound closure ratio decreased by 29% (A549) and 22% (A549/DDP), respectively, indicating that **RuIQ-5** could effectively inhibit the migration of both A549 and A549/DDP cells even at a low dosage.

2.4. Cytotoxicity on 3D multicellular tumor spheroids (MCTSs)

3D multicellular tumor spheroid (MCTS) model has received increasing interest in recent years, since it can realistically mimics the extracellular matrix (ECM) and the *in vivo* situations and therefore have been widely applied in the drug discovery process [42]. In particular, research based on MCTSs can gain insights into the metabolic and proliferative gradients in tumors which contribute to the therapeutic challenges of cancers, such as altered responsiveness of chronically hypoxic tumor cells, and resistance to multiple apoptosis-inducing agents. MCTSs with diameters of approximately 400 μm resemble solid tumors in terms of pathophysiological conditions, such as specific hypoxic areas in the center of a tumor, and gradient proliferation rates of tumor cells

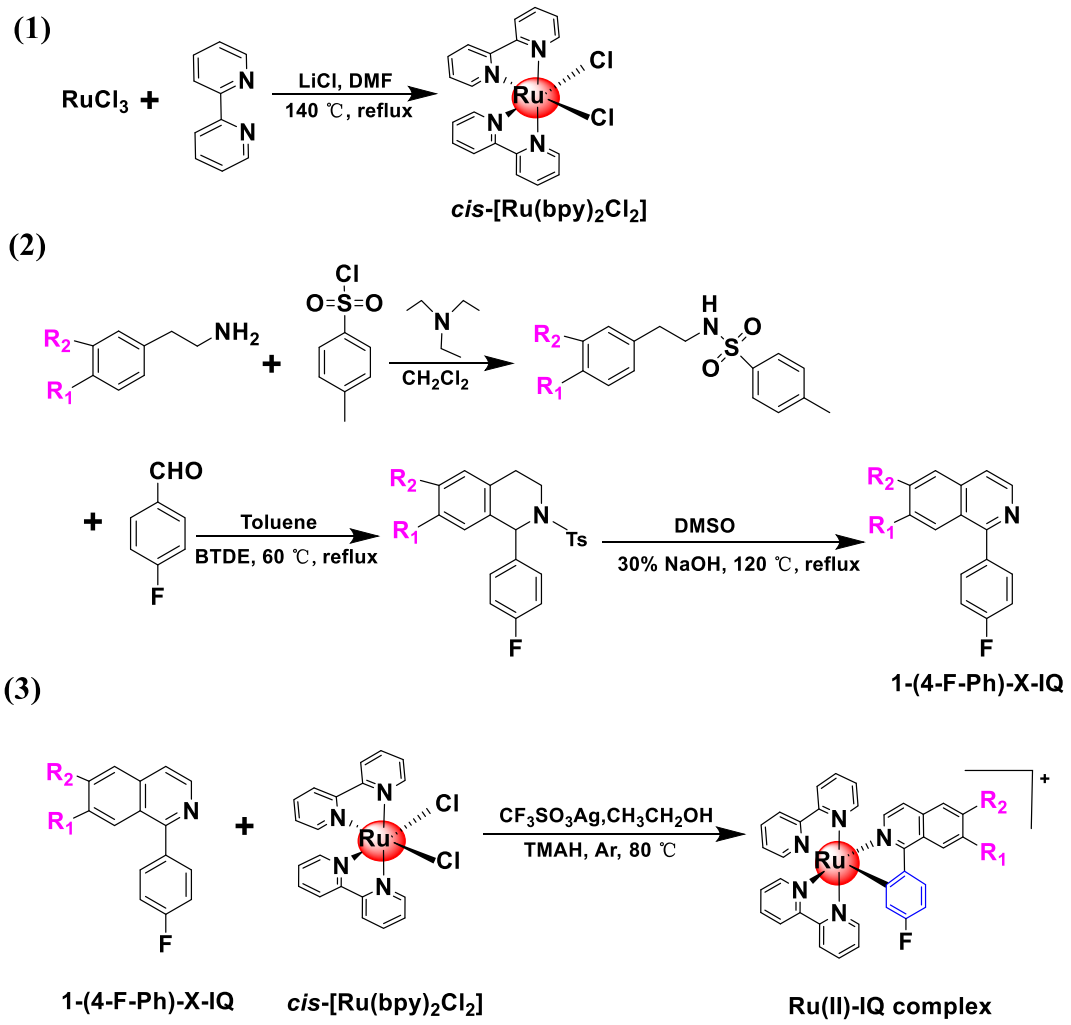

complex	R1	R2
RuIQ-3	H	H
RuIQ-4	OCH_3	H
RuIQ-5	OCH_3	OCH_3

Scheme 1. The synthetic routes of precursor *cis*-[Ru(bpy)$_2$Cl$_2$], ligands 1-(4-F-Ph)-IQ, 1-(4-F-Ph)-7-OCH$_3$-IQ, and 1-(4-F-Ph)-6,7-(OCH$_3$)$_2$-IQ, and the cyclometalated Ru(II)-IQ complexes **RuIQ-3**, **RuIQ-4** and **RuIQ-5**.

[43,44]. Therefore, we tested the cytotoxicities of the Ru(II)-IQ complexes (**RuIQ-3**, **RuIQ-4**, **RuIQ-5**) against A549 and A549/DDP MCTSs with diameters of approximately 400 μm [42]. As shown in Fig. 3(A), the IC_{50} value of cisplatin against A549 MCTSs was 62 μM and it even exceeded 200 μM in A549/DDP MCTSs. In contrast, the IC_{50} values of the Ru(II)-IQ complexes against A549 MCTSs (**RuIQ-3**: 4.9 μM, **RuIQ-4**: 4.2 μM, **RuIQ-5**: 2.8 μM) and A549/DDP MCTSs (**RuIQ-3**: 5.2 μM, **RuIQ-4**: 4.3 μM, **RuIQ-5**: 2.9 μM) were much lower, indicating that the cyclometalated Ru(II)-IQ complexes can efficiently inhibit tumor growth and overcome drug resistance.

Meanwhile, we monitored the growth rate of MCTSs by administering different concentrations of **RuIQ-5** (Fig. S14). MCTSs were treated with **RuIQ-5** (1.0, 2.0, 4.0 μM) for 72 h, then 50% of the plated medium was replaced with fresh medium every two days. In this way, loss or disruption of the MCTSs could be avoided [40]. As shown in Fig. S14, the growth of MCTSs was significantly delayed by **RuIQ-5** after 14 days. The size of the **RuIQ-5** treated MCTSs were apparently smaller than the cisplatin treated and untreated MCTSs, which means the proliferation of A549 and A549/DDP cells was significantly inhibited by **RuIQ-5**. Moreover, **RuIQ-5** inhibited the growth of MCTSs in a clear-cut dose dependent manner (Fig. S14), thus confirming the antitumor activity of **RuIQ-5**.

To visualize the antitumor effectiveness of **RuIQ-5**, MCTSs were treated with 1.0, 2.0, and 4.0 μM of **RuIQ-5** respectively, after which the spheroids were stained with calcein AM (staining the living cells) and propidium iodide (PI, staining the dead cells), respectively. As shown in Fig. 3(B), A549 or A549/DDP cells in untreated MCTSs emitted steady green fluorescence, indicating that the cells were living. In contrast, when MCTSs were treated with 1.0, 2.0, and 4.0 μM of **RuIQ-5** the green fluorescence was significantly weakened and the bright-red fluorescence gradually increase, indicating that cells had been damaged. In addition, the red fluorescence was dependent on the dose of **RuIQ-5**. These results

Table 1
IC_{50} values (μM) of Ru(II)-IQ complexes (**RuIQ-3**, **RuIQ-4**, **RuIQ-5**) against the selected human cancer cell lines.[a]

Complex	IC_{50} (μM)					RF[b]	SI[c]
	A549	A549/DDP	HepG2	MCF-7	HBE		
cis-[Ru(bpy)$_2$Cl$_2$]	>200	>200	>200	>200	–	–	–
1-(4-F-Ph)-IQ	179.6 ± 6.3	>200	196.4 ± 6.9	>200	>200	–	–
1-(4-F-Ph)-7-OCH_3-IQ	168.7 ± 6.4	>200	192.2 ± 5.1	191.6 ± 6.3	>200	–	–
1-(4-F-Ph)-6,7-(OCH_3)$_2$-IQ	152.5 ± 5.8	>200	185.8 ± 5.4	182.6 ± 5.1	> 200	–	–
RuIQ-3	4.5 ± 0.5	4.9 ± 0.5	8.4 ± 0.6	7.9 ± 0.7	25.2 ± 1.6	1.09	5.14
RuIQ-4	3.8 ± 0.4	4.1 ± 0.3	7.8 ± 0.5	7.2 ± 0.5	23.8 ± 2.1	1.08	5.80
RuIQ-5	2.2 ± 0.3	2.3 ± 0.2	7.2 ± 0.4	6.8 ± 0.5	18.3 ± 0.1	1.04	7.96
Cisplatin	15.6 ± 1.1	48.8 ± 2.1	18.4 ± 1.5	21.5 ± 1.3	19.8 ± 1.2	3.13	1.27

[a] Cell viability was determined by MTT assay after ligands or complexes treatment with cells for 48 h.
[b] RF (resistant factor) = IC_{50} (A549/DDP)/IC_{50} (A549).
[c] SI (selectivity index) = IC_{50} (HBE)/IC_{50}(A549/DDP).

revealed that **RuIQ5** could inhibit the growth of MCTSs and induce tumor cell death.

2.5. Fish embryo acute toxicology test (FET).

Embryo-larval zebrafish has served as a useful model for toxicology and drug development studies. More than just an alternative to mouse, zebrafish model has emerged as a complement to mammals in toxicological studies that the toxicological results can predict the effects in mammals [45–47]. In this work, zebrafish embryos were used as a vertebrate model for the *in vivo* toxicity evaluation of the newly synthesized Ru(II)-IQ complex **RuIQ-5**.

As shown in Fig. 4A, after exposure to **RuIQ-5** at concentrations less than 13.6 μg/mL (16.0 μM) for 72 h, all zebrafish embryos grew into juveniles, with an acceptable cumulative hatch rate of 80% (Fig. 4B). And, the lethality rate was lower than 20% even after 96 h (Fig. 4C). However, when the concentration of **RuIQ-5** increased to 13.6 μg/mL, some zebrafish embryos developed abnormally with a noticeable spinal curvature (Fig. 4A). When the **RuIQ-5** concentration was increased to 27.2 μg/mL (32.0 μM), the hatch rate of zebrafish embryo decreased to less than 20% at 72 h, and all the embryos died at 96 h. These results indicated that **RuIQ-5** (less than 13.6 μg/mL) possessed little *in vivo* toxicity in zebrafish embryos, which demonstrated an acceptable safety profile. Therefore, it is expected that **RuIQ-5** could be developed as a low-toxicity agent against lung cancer. Hence, further studies (which were discussed in later sections) were performed to elucidate mechanism underlying the antitumor effect and the reversal of cisplatin resistance of **RuIQ-5** in A549/DDP cells.

2.6. Lipophilicity and cellular uptake

To evaluate the ability of Ru(II)-IQ complexes entering cells, their lipophilicity, expressed as oil–water partition coefficient (log$P_{o/w}$), was determined by the shake-flask method using inductively coupled plasma mass spectrometry (ICP-MS). As shown in Fig. 5A, the log$P_{o/w}$ values were in the following order: **RuIQ-5** (1.25) > **RuIQ-4** (1.10) > **RuIQ-3** (0.65) > cisplatin (-4.53), which was in accordance with the order of cellular metal content (Fig. 5B), confirming that a higher lipophilicity of Ru(II)-IQ complexes enhanced their tumor penetration and cellular uptake. It's worth noting that there was no significant difference in the uptake of Ru(II)-IQ complexes between A549 and A549/DDP cell lines, in contrast, the uptake of cisplatin by A549/DDP was significantly lower than A549, implying that the ability of the Ru(II)-IQ complexes (**RuIQ-3**, **RuIQ-4**, **RuIQ-5**) to reverse drug resistance may be related to their efficient penetration into target tumor cells [48]. Besides, the subcellular distribution of **RuIQ-5** in A549 and A549/DDP cells was further determined by ICP-MS with cisplatin as a control (Fig. 5C). As shown in Fig. 5C, **RuIQ-5** complexes were predominantly accumulated in the nucleus and only a small fraction of the complexes were found in mitochondria and cytoplasm, implying that **RuIQ-5** might affect genome replication and gene expression. In contrast, cisplatin was mainly distributed in the cytoplasm of A549/DDP cells instead of the nucleus (Fig. 5C). These results suggest that **RuIQ-5** is a highly cell-permeable, nucleus-targeting Ru(II) complex, which is similar to other cyclometalated Ru(II) complexes reported earlier such as [Ru(bpy)(phpy)(dppz)]$^+$ [49], [Ru(dmb)$_2$(1-Ph-βC)](PF_6) [50], [Ru(bpy)$_2$(1-Ph-βC)](PF_6) [50], [Ru(bpy)$_2$(1-Ph-IQ)]$^+$ [39], and [Ru(phen)$_2$(1-Ph-IQ)]$^+$ [39].

In general, drug molecules cross cell membrane and reach cytoplasm through adenosine-5′-triphosphate (ATP)-dependent active transport or nonenergy-dependent passive diffusion [51]. To evaluate the internalization pathway of **RuIQ-5** complexes, A549 and A549/DDP cells were treated with **RuIQ-5** at low temperature (4 °C) or pretreated with sodium azide (NaN_3) in combination with 2-Deoxy-D-glucose (2-DOG), a commonly used strategy to block ATP-dependent active transportation. As shown in Fig. 5D, both low temperature and NaN_3/2-DOG could strongly inhibit the cellular uptake of **RuIQ-5**, confirming that **RuIQ-5**

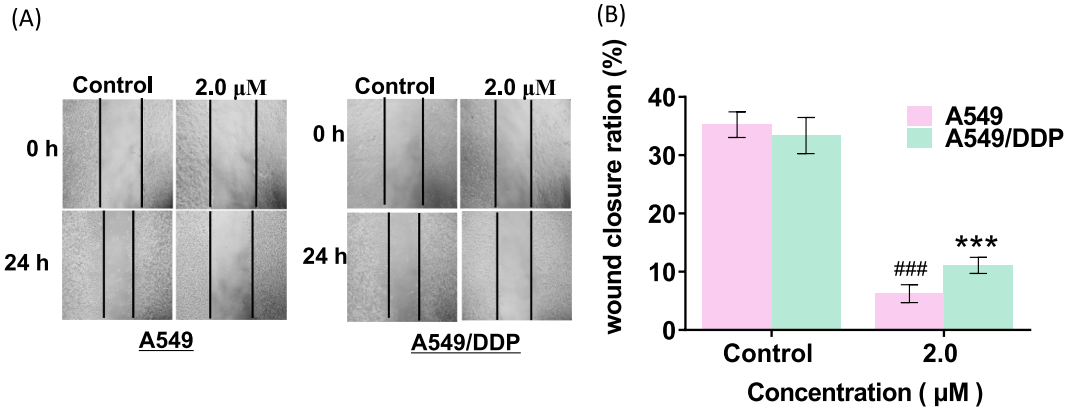

Fig. 2. Wound healing assay of A549 and A549/DDP cells treated with or without **RuIQ-5** for 24 h. (A) Typical images were taken at 0 and 24 h. (B) Quantification of microscope images. Data are quoted as mean ± SD of three replicates. × ± s, n = 3. $^{###}P < 0.001$ vs A549 control, $^{***}P < 0.001$ vs A549/DDP control.

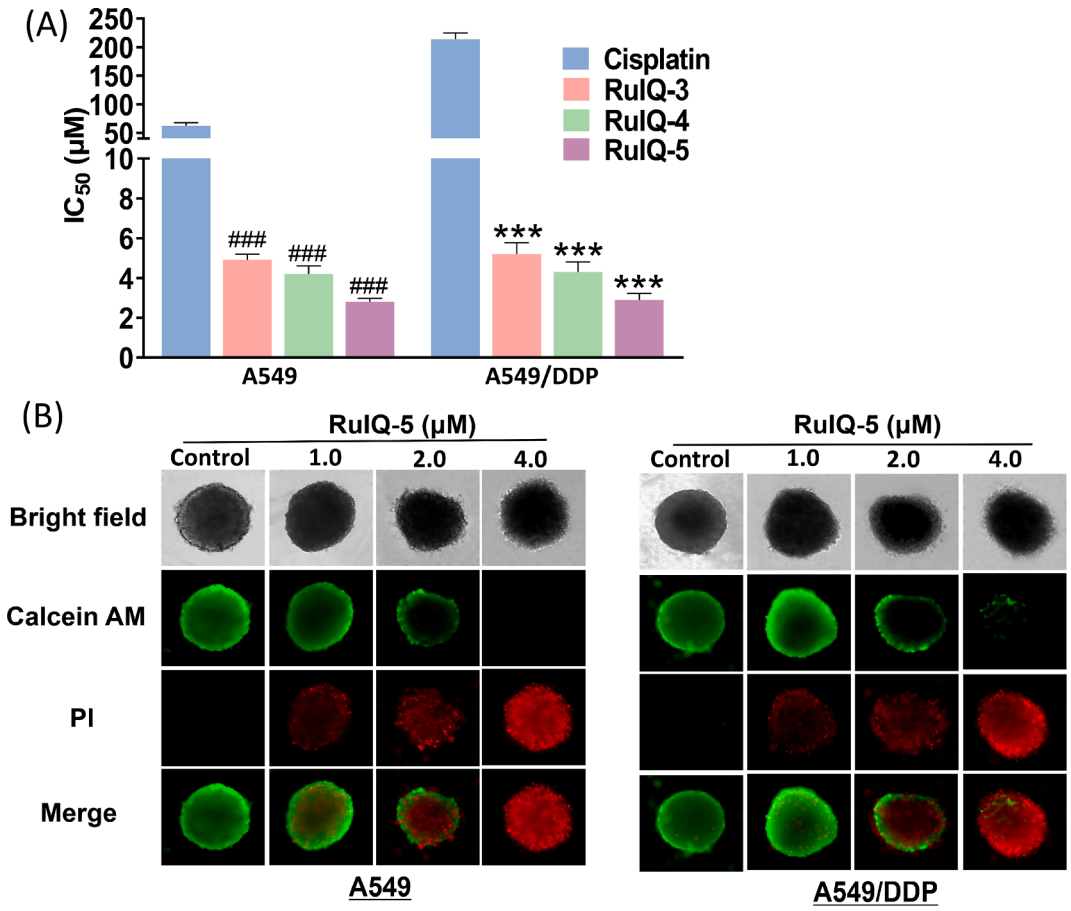

Fig. 3. Cytotoxicity assay of 3D MCTSs model. (A) IC_{50} values of cisplatin and Ru(II)-IQ complexes (**RuIQ-3**, **RuIQ-4**, **RuIQ-5**) against A549 and A549/DDP MCTSs after 72 h drug exposures. (B) Calcein AM and PI dual-staining of MCTSs treated by indicated concentrations of **RuIQ-5** for 72 h. × ± s, n = 3. $^{###}P < 0.001$ vs A549 control, $^{***}P < 0.001$ vs A549/DDP control.

enters A549 and A549/DDP cells in an energy-dependent manner. Endocytosis is the most common energy-dependent pathway. Therefore, we further investigated the internalization pathway of **RuIQ-5** with two endocytosis inhibitors nystatin (inhibitor of clathrin-mediated endocytosis) and sucrose (inhibitor of lipid raft-mediated endocytosis) [52]. Similarly, cellular uptake level of **RuIQ-5** was also reduced in both the nystatin and sucrose treatment groups. These results suggested that **RuIQ-5** complexes were actively transported into A549 and A549/DDP cells mainly through endocytosis.

2.7. RuIQ-5 triggers inhibition of DNA replication and DNA damage

Since **RuIQ-5** accumulated mostly in the cell nucleus, we tested the inhibitory effect of **RuIQ-5** on DNA replication by carrying out an antiproliferation assay [49]. 5-ethynyl-2′-deoxyuridine (EdU) is a thymidine analogue that can be integrated into DNA as a red fluorescent marker in active cell proliferation, thereby it was used in this assay [53]. As shown in Fig. 6, a large amount of red fluorescence was observed in the nucleus of A549 and A549/DDP cells in the control groups, indicating the newly replicated DNA. In contrast, the amount of newly replicated DNA was decreased significantly in the cells treated with different concentrations of complex **RuIQ-5** (1.0, 2.0, 4.0 μM). When the concentration of **RuIQ-5** reached 4.0 μM, the synthesis of DNA was almost completely inhibited. These results suggested that complex **RuIQ-5** could effectively inhibit the DNA amplification in A549 and A549/DDP cells.

DNA damage can lead to inhibition of its replication, failure to repair damaged DNA may induce cell death. Therefore, DNA damage is considered to be a marker of apoptosis [54,55]. Single cell gel electrophoresis (SCGE), also known as comet assay, is an efficient and rapid method for detecting DNA damage that the damage degree is directly reflected by the length of comet tails [56,57]. To determine whether **RuIQ-5** complexes can induce DNA damage or not, comet assay was performed. As shown in Fig. 7A, both A549 and A549/DDP cells in the control did not display comet tail artifact, indicating that the DNA in untreated cells was intact. After incubation with 1.0 μM of **RuIQ-5** for 24 h, both A549 and A549/DDP cells exhibited legible comet tails, indicating that mild DNA damage has occurred. When the concentration of **RuIQ-5** was increased to 4 μM, long and thick comet tails could be observed, suggesting that severe DNA damage has occurred. The length of comet tails was then quantified by Image J software and shown in Fig. 7B. These results suggested that **RuIQ-5** could induce DNA damage in a dose-dependent manner, which might be responsible for the inhibition of DNA amplification.

DNA damage can directly affect DNA replication, transcription, and lead to cell cycle arrest [58]. To investigate the effects of **RuIQ-5** on cell cycle distribution, A549 and A549/DDP cells were treated with **RuIQ-5** (1.0, 2.0, 4.0 μM) for 24 h and analyzed by flow cytometry. The results in Fig. S15 showed that treatment of A549 and A549/DDP cells with **RuIQ-5** significantly increased the percentages of cells in both the S and G2/M phases in a concentration-dependent manner. For instance, the percentage of A549/DDP cells in G2/M phase was 6.15% before treatment, and increased to 10.83% and 18.67% when treated with 1.0 and 4.0 μM of **RuIQ-5**, respectively. These findings denoted that, like other cyclometalated Ru(II)-IQ complexes [39], **RuIQ-5** could induce cell cycle arrest at S and G2/M phases in A549 and A549/DDP cells.

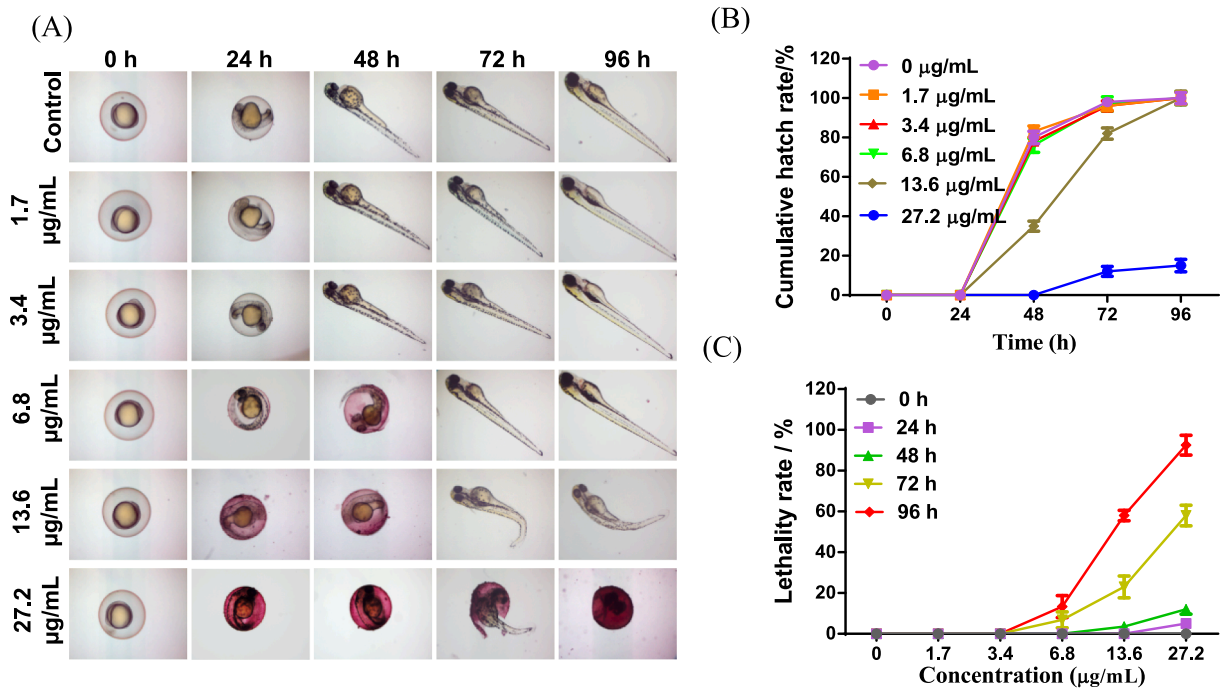

Fig. 4. Toxicity assessment of **RuIQ-5** in developing zebrafish embryos. (A) Toxicity of **RuIQ-5** to zebrafish embryos at various concentrations (1.7, 3.4, 6.8, 13.6, 27.2 μg/mL) within 96 h on a 4 × objective lens in the microscope. (B) Cumulative hatch rate of zebrafish embryos in the presence/absence of **RuIQ-5** at various concentrations (0, 1.7, 3.4, 6.8, 13.6, 27.2 μg/mL) every 24 h. (C) Lethality rate of zebrafish embryos in the presence/absence of **RuIQ-5** at different concentrations (0, 1.7, 3.4, 6.8, 13.6, 27.2 μg/mL) every 24 h.

2.8. RuIQ-5 induces apoptosis in A549 and A549/DDP cells

Cell cycle arrest and DNA damage may result in cell division blockage and apoptosis [59]. Apoptosis often causes cell morphological changes, such as nuclear condensation and fragmentation, and formation of apoptotic bodies [60]. A549 or A549/DDP cells were treated with **RuIQ-5** (1.0, 2.0, 4.0 μM) for 24 h, and the **RuIQ-5**-induced morphological changes of cells were observed by Hoechst33342 fluorescent staining. As shown in Fig. S16A and 16B, after staining with Hoechst 33342, nuclear condensation and apoptotic bodies were observed in the **RuIQ-5**-treated cells. Moreover, cell apoptosis was evaluated by acridine orange/ethidium bromide (AO/EB) dual-staining. As shown in Fig. S16C, in the control groups, A549 and A549/DDP cells with normal morphology were labeled homogeneously with green fluorescence. In contrast, clearly morphological features of apoptosis and apoptotic cells showing orange or red fluorescence were observed in the **RuIQ-5** treatment groups. These preliminary results indicated that **RuIQ-5** could induce apoptosis in both A549 and A549/DDP cells.

In order to further quantitatively analyze the cell death-inducing ability of **RuIQ-5**, annexin V-fluorescein isothiocyanate (FITC)/PI staining was performed and analyzed using flow cytometry. Fig. 8A and 8B showed that pre-incubation of A549 or A549/DDP cells with complex **RuIQ-5** of different concentrations (1.0, 2.0, 4.0 μM) for 24 h enhanced the percentage of apoptotic cells. Specifically, the proportion of the **RuIQ-5** treated cells in early apoptosis and late apoptosis/necrosis was increased significantly in a dose-dependent manner. Western blot was used to detect apoptosis-related proteins to confirm the occurrence of apoptosis. As shown in Fig. 8C, **RuIQ-5** significantly increased the expression level of cleaved caspase-3, -8, -9, and poly (ADP-ribose) polymerase (PARP) in both A549 and A549/DDP cells in a concentration-dependent manner. These results undoubtedly demonstrated that **RuIQ-5** could induce apoptosis in A549 and A549/DDP cells [61,62].

2.9. RuIQ-5 induces mitochondrial dysfunction

Mitochondrial dysfunction is involved in apoptotic cell death [49]. Apoptosis-inducing factors released by mitochondrion, such as cytochrome *c* play an important role in the initiation of apoptosis [63–67]. The decline of mitochondrial membrane potential (MMP) is an early marker of apoptosis. We used 5,5′,6,6′-Tetrachloro-1,1′,3,3′-tetraethylbenzimidazolylcarbocyanine iodide (JC-1) dye to detect the decline of MMP in A549 and A549/DDP cells after **RuIQ-5** treatment. As shown in Fig. 9A, after treatment of cells with **RuIQ-5** (1.0, 2.0, 4.0 μM) for 24 h, the green fluorescence was significantly enhanced while the intensity of red fluorescence was weakened, indicating a decrease in MMP. The changes of MMP were quantitatively analyzed by flow cytometry, as shown in Fig. 9B and Fig. S17, the MMP decline in A549 and A549/DDP cells was dependent on the concentration of **RuIQ-5**.

In addition, western blot analysis was performed to confirm the mitochondrial pathways in apoptosis induced by **RuIQ-5** treatment. The results in Fig. 9C indicated that the ratios of Bcl-2/Bax and Bcl-xl/Bad were decreased, the apoptosis inducing factor, cytochrome *c* was released into the cytosol. The increase of cytosolic cytochrome *c* was dependent on the dosage of **RuIQ-5** (Fig. 9C). These results further confirmed that **RuIQ-5** could induce mitochondrial dysfunction, which contributes to apoptosis in A549 and A549/DDP cells.

2.10. RuIQ-5 stimulates intracellular ROS accumulation

It has been demonstrated that ROS can induce apoptosis via a variety of mechanisms. For example, increased ROS can activate the intrinsic pathway of apoptosis by stimulating the depolarization of MMP [68]. However, the majority of cancer cells can remain viable in the presence of intrinsic oxidative stress, thereby enabling them to avoid apoptosis and become resistant to many chemotherapeutic drugs [69,70]. In order to elucidate the underlying mechanism of **RuIQ-5**-induced apoptosis in A549 and A549/DDP cells, we investigated their cellular ROS levels using 7-dichlorodi-hydrofluorescein diacetate (DCFH-DA) fluorescent

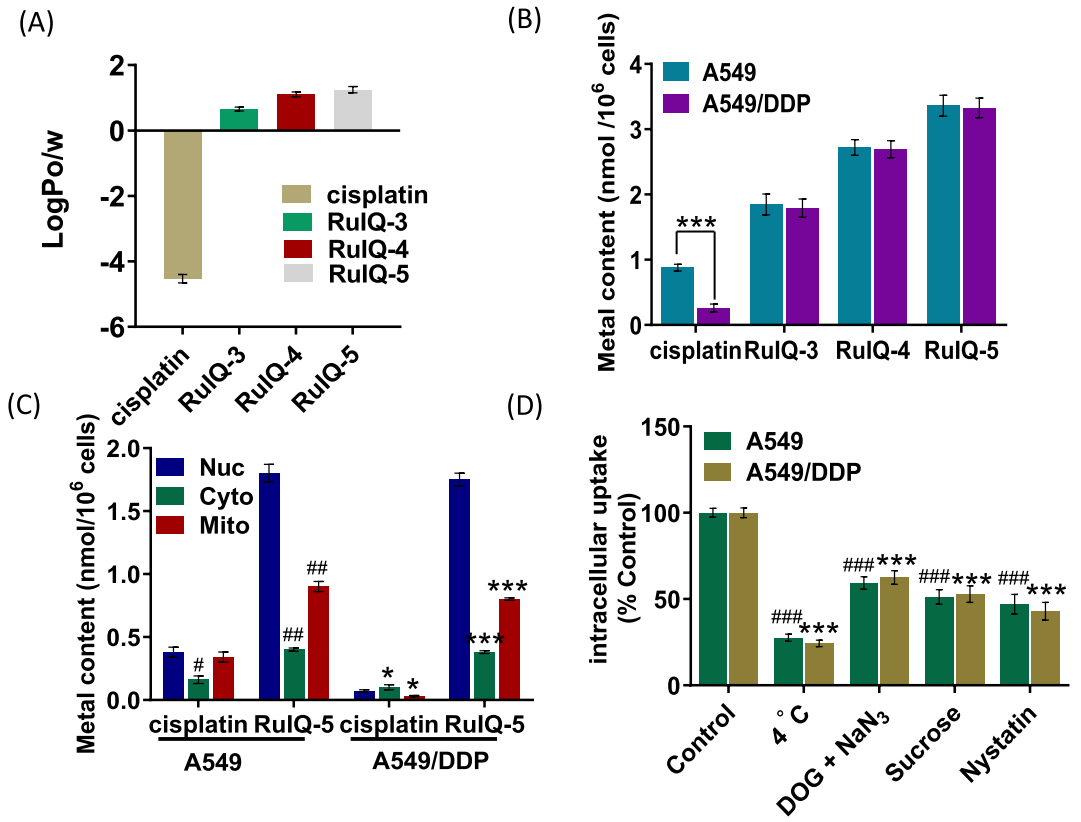

Fig. 5. Lipophilicity and cellular uptake of cisplatin and Ru(II)-IQ complexes (**RuIQ-3**, **RuIQ-4**, **RuIQ-5**) in A549 and A549/DDP cells. (A) Log$P_{o/w}$ values of cisplatin and Ru(II)-IQ complexes. (B) Cellular Ruthenium or platinum contents determined in A549, A549/DDP cells after 24 h incubation with cisplatin, **RuIQ-3**, **RuIQ-4**, or **RuIQ-5** at 2.0 μM, respectively. × ± s, n = 3. $^{***}P < 0.01$ vs cisplatin treatment group of A549. (C) Subcellular distribution of ruthenium or platinum contents in A549 and A549/DDP cells after incubation with cisplatin or **RuIQ-5** at 2.0 μM for 24 h. x ± s, n = 3. $^{\#}P < 0.05$, $^{\#\#}P < 0.01$ vs A549 nucleus, $^{*}P < 0.01$, $^{***}P < 0.001$ vs A549/DDP nucleus. (D) Intracellular uptake of **RuIQ-5** in A549 and A549/DDP cells under different endocytosis-inhibited conditions at 2.0 μM. × ± s, n = 3. $^{\#}P < 0.05$, $^{\#\#}P < 0.01$ vs A549 control, $^{**}P < 0.01$, $^{***}P < 0.001$ vs A549/DDP control.

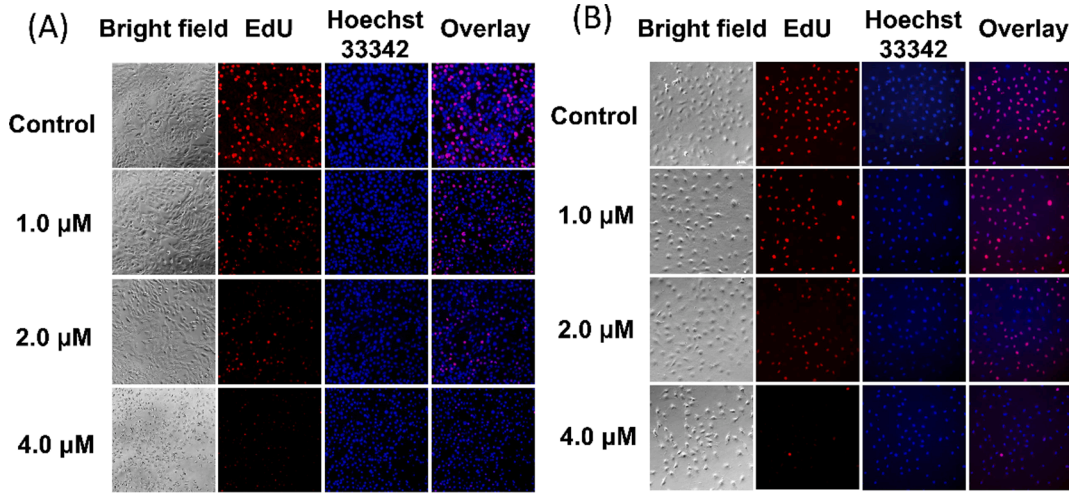

Fig. 6. Anti-proliferation assay of A549 and A549/DDP cells treated by EdU after 1.0, 2.0 4.0 μM of **RuIQ-5** treatment for 12 h. (A) Anti-proliferation assay in A549 cells. (B) Anti-proliferation assay in A549/DDP cells.

probe. It was observed that, prior to **RuIQ-5** treatment, the intensity of DCFH-DA fluorescence in A549/DDP cells was stronger than that of A549 cells, which might be associated with the drug resistance in A549/DDP cells [70]. Furthermore, as shown in Fig. S18, compared with the control group, both A549 and A549/DDP cells exhibited obvious green fluorescence when treated with **RuIQ-5** at 1.0, 2.0, 4.0 μM for 12 h, indicating an increase in the cellular ROS level. A similar result was also obtained by flow cytometry (Fig. 10A). The results in Fig. 10A and B revealed that the increase in the cellular ROS levels as a result of **RuIQ-5** treatment was dependent on the dose (1.0, 2.0, 4.0 μM).

To further explore the role of ROS in triggering apoptosis, two ROS scavengers, NAC and GSH, were used. As shown in Fig. 10C, the production of cellular ROS was significantly reduced in the **RuIQ-5**/NAC and **RuIQ-5**/GSH treatment groups, in contrast to the cells treated by

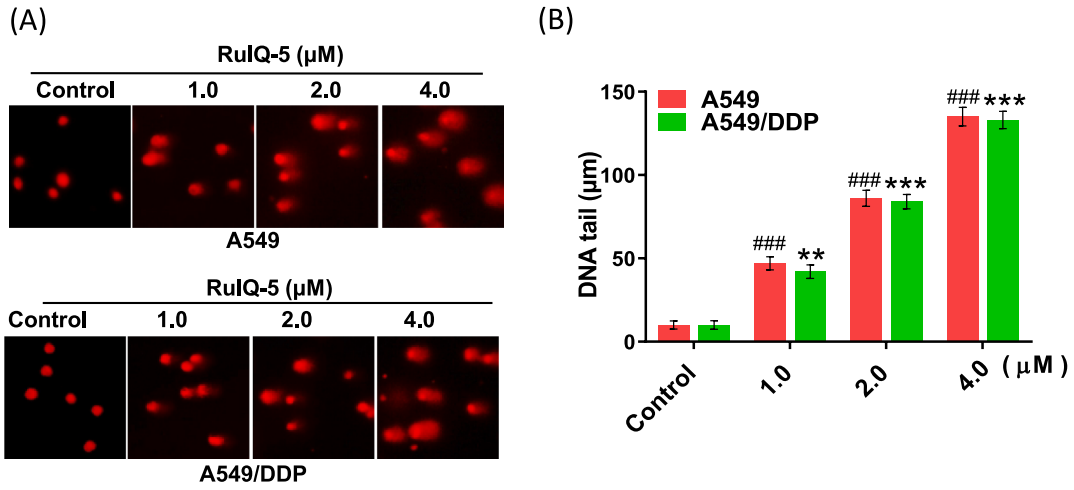

Fig. 7. DNA damage was examined by comet assay. (A) A549 and A549/DDP cells were treated with various concentrations (1.0, 2.0, 4.0 μM) of **RuIQ-5** for 24 h, and DNA fragmentation was examined by comet assay. (B) Quantification of DNA tails in the comet assay. The length of DNA tails in microscopy images was quantified by Image J. × ± s, n = 3. $^{\#\#}P < 0.01$, $^{\#\#\#}P < 0.001$ vs A549 control, $^{**}P < 0.01$, $^{***}P < 0.001$ vs A549/DDP control.

RuIQ-5 alone. Moreover, NAC or GSH pretreatment led to increased A549 and A549/DDP cell viability as well (Fig. 10D). Altogether, these results revealed that activation of ROS generation by **RuIQ-5** played an important role in inducing apoptosis in A549 and A549/DDP cells.

2.11. Akt/GSK-3β/Fyn signaling pathway was involved in RuIQ-5-induced apoptosis

Nrf2, a key transcriptional regulator of antioxidant and anti-inflammatory enzymes, is abundantly expressed in cancer cells [71]. In NSCLC patients, Nrf2 is usually deregulated at both the transcriptional level and protein level [72]. It has been shown that GSK-3β, a subtype of GSK3, can regulate Fyn-mediated export and degradation of Nrf2 in the nucleus [8–10]. GSK-3β phosphorylates Fyn, which subsequently phosphorylates and activates Nrf2, leading to the promotion of apoptosis by enhanced Nrf2 degradation; however, activated Akt can phosphorylate the Ser9 residue of GSK-3β, thereby inhibiting GSK-3β activity and protecting cells from apoptosis [73,74]. The reversal of tumor drug resistance by **RuIQ-5** may be related to the Akt/GSK3β/Fyn signaling pathway. Hence, we evaluated the effect of **RuIQ-5** on the expression levels of Akt and GSK3β in both A549 and A549/DDP cells. As shown in Fig. 11A, the expression of p-Akt, p-GSK3β, and Nrf2 in A549/DDP cells was higher than that in A549 cells, while p-Fyn level in A549/DDP cells was lower than that in A549 cells. After treatment with **RuIQ5**, in A549 cells, p-Akt and total Nrf2 decreased, but GSK3β and p-Fyn did not change much. However, in A549/DDP cells, **RuIQ5** treatment downregulated the expression of p-Akt and p-GSK3β, while GSK3β and p-Fyn levels were increased . In addition, **RuIQ5** treatment resulted in a decrease in the levels of nucleus Nrf2 and its downstream resistance-associated proteins MRP1 and HO-1 in A549/DDP cells in a concentration-dependent manner (Fig. 11B). The above results indicated that RuIQ5 could reverse the drug resistance in A549/DDP cells through regulation of Akt/GSK3β/Fyn pathway.

The localization of Nrf2 is essential for its biological function [4,6]. The effects of **RuIQ-5** on the distribution of Nrf2 in cells were observed by immunofluorescence staining, with PI3K inhibitor LY294002 used as a positive control. We found that Nrf2 was mainly expressed in the cytoplasm of A549 cells, while Nrf2 fluorescence was significantly enhanced in A549/DDP cells, with increased expression in the nucleus (Fig. 11C and 11D). **RuIQ-5** treatment reduced the fluorescence intensity of Nrf2 in A549/DDP cells and hindered its nuclear expression (Fig. 11D). However, in A549 cells, the ruthenium complex **RuIQ-5** had no significant effect on the nuclear translocation of Nrf2.

Taken together, regulation of Akt/GSK3β/Fyn signaling pathway by **RuIQ-5** treatment led to downregulation of Nrf2, which could improve the sensitivity of A549/DDP cells to antineoplastic drugs by reversal of drug resistance in cells.

3. Conclusions

In this study, three Ru(II)-IQ complexes $[Ru(bpy)_2(1\text{-}(4\text{-F-Ph})\text{-IQ})]^+$ (**RuIQ-3**), $[Ru(bpy)_2(1\text{-}(4\text{-F-Ph})\text{-7-}OCH_3\text{-IQ})]^+$ (**RuIQ-4**), and $[Ru(bpy)_2(1\text{-}(4\text{-F-Ph})\text{-6,7-}(OCH_3)_2\text{-IQ})]^+$ (**RuIQ-5**) were synthesized, characterized and evaluated biologically. Among them, **RuIQ-5** exhibited the highest cellular uptake and thus displayed the most potent anti-proliferation activities against both A549 and A549/DDP cells. Studies on the intracellular distribution showed that **RuIQ-5** was mainly distributed in the nucleus other than cytoplasm upon absorption by A549/DDP cells. Cytotoxicity assays based on 3D MCTSs tumor spheroid models further demonstrated the ability of Ru(II)-IQ complexes to overcome multicellular drug resistance. Moreover, **RuIQ-5** exhibited low toxicity both towards normal HBE cells *in vitro* and zebrafish embryos *in vivo*, displaying a promising safety profile. Further, molecular mechanism studies revealed that **RuIQ-5** could induce ROS-mediated apoptosis in A549 and A549/DDP cells through mitochondrial dysfunction, DNA damage, and cell cycle arrest in S and G2/M phases (Fig. 12). Studies also showed that **RuIQ-5** could reverse the drug resistance of A549/DDP cells through regulation of Akt/GSK3β/Fyn signaling pathway (Fig. 12). Based on these findings, we believe that Ru(II)-isoquinoline complexes could be developed as efficient Nrf2 inhibitors and overcome the cisplatin resistance in NSCLC.

4. Experimental section

4.1. Materials and general methods

All reagents and solvents were purchased commercially and used without further purification. DMSO, 3-(4,5-dimethylthiazol-2-yl)-2,5-diphenyltetrazolium bromide (MTT), Hoechst 33342, phosphate buffered saline (PBS), 5,5′6,6′-tetrachloro-1,1′,3,3′-tetraethylimidacarbocyanine iodide (JC-1), 2,7-Dichlorodi-hydrofluorescein diacetate (DCFH-DA), Annexin V-FITC apoptosis detection kit, QuantiPro™ BCA assay kit, and ECL™ Start Western blotting detection reagent were purchased from Sigma-Aldrich (St. Louis, MO, USA). Cell mitochondria isolation kit, BeyoClick EdU-594 cell proliferation assay kit, calcein AM (excitation at 488 nm, emission at 515 nm), propidium iodide (PI) (excitation at 535 nm, emission at 617 nm), and CellTiter-Lumi™ Plus luminescent cell viability assay kit were purchased from Beyotime

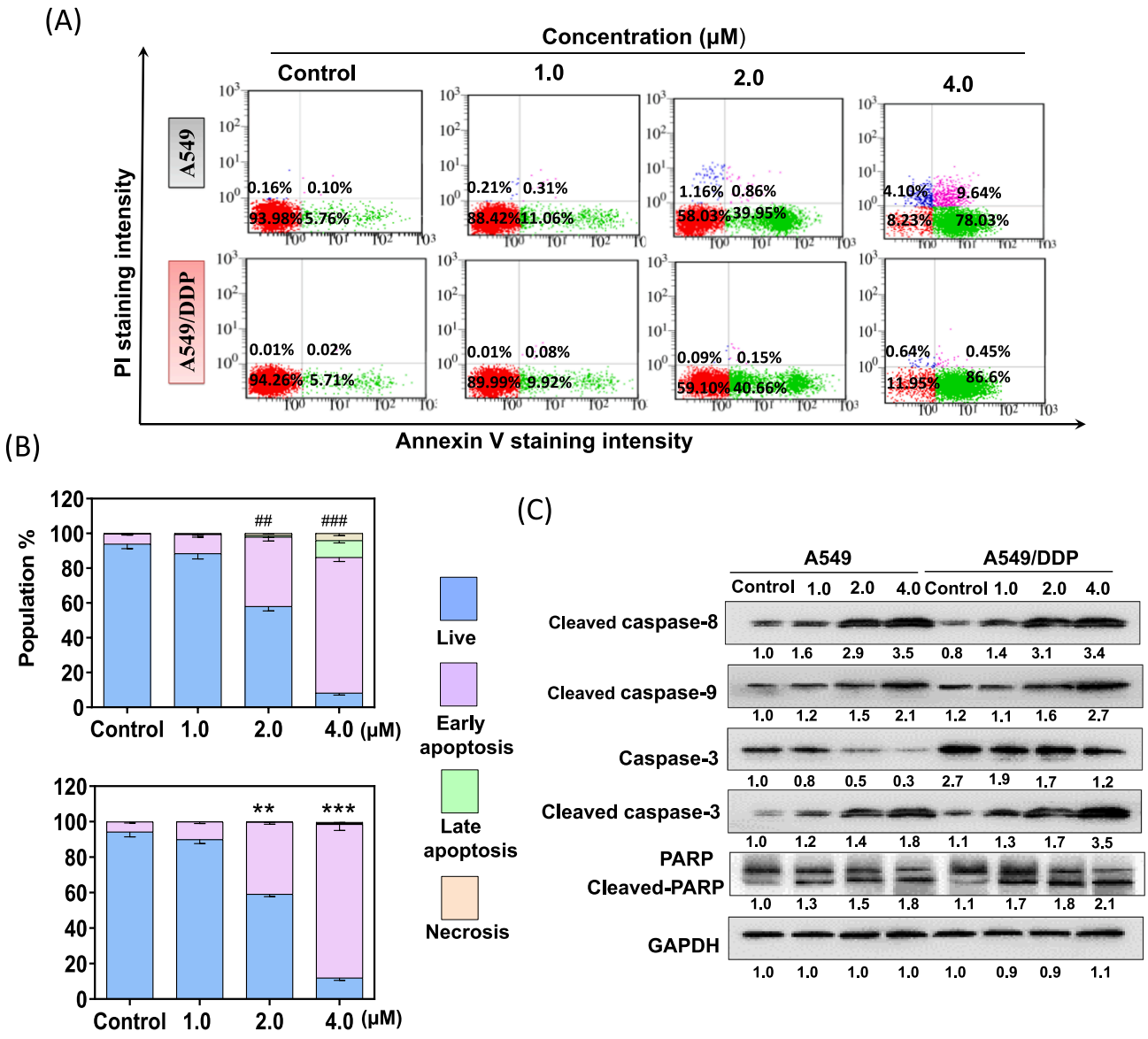

Fig. 8. Ru(II)-IQ complex **RuIQ-5** induced A549 and A549/DDP cells apoptosis. (A) A549 and A549/DDP cells apoptosis was detected by annexin V/PI assay after co-incubation with 1.0, 2.0, 4.0 μM of **RuIQ-5** for 24 h. (B) Populations for A549, A549/DDP cells in four stages. × ± s, n = 3. $^{\#\#}P < 0.01$, $^{\#\#\#}P < 0.001$ vs A549 control, $^{**}P < 0.01$, $^{***}P < 0.001$ vs A549/DDP control. (C) The expression levels of caspase-3, PARP and cleaved caspase-3/8/9 and PARP were evaluated in a concentration-dependent manner with **RuIQ-5** (1.0 2.0 4.0 μM) treatment for 24 h. GAPDH was used as internal control.

(Shanghai, China). Ruthenium standard solution was purchased from Aladdin Chemistry Co. Ltd (Shanghai, China). Primary and secondary antibodies were purchased from Cell Signaling Technology, Inc. CometAssay® reagent kit was purchased from Trevigen (Gaithersburg, MD, USA). Dulbecco's Modified Eagle Medium (DMEM) and fetal bovine serum (FBS) were obtained from HyClone.

Protein bands were visualized using ChemiDoc™ XRS + Imaging System (Bio-Rad, USA). Elemental microanalyses (C, H, and N) were performed using a Perkin–Elmer 240Q elemental analyzer. Electrospray ionization mass spectrometry (ESI-MS) was recorded on Agilent LC-MS6430B Spectrometer. ^{1}H NMR spectra were recorded on a Bruker AVANCE 400 spectrometer (400 MHz) at room temperature. UV–visible (UV–Vis) and emission spectra were measured on Perkin–Elmer Lambda-850 spectrophotometer at 25 °C. Flow cytometry was performed using an EPICS® XL-MCL flow cytometer (BECKMAN COULTER, USA). Fluorescence observation was performed by Ti-E inverted microscope (Nikon, Japan). Microplate was read by Infinite M200 Pro multimode microplate reader (Tecan, Switzerland).

4.2. Synthesis and characterization

1-(4-F-Ph)-IQ, 1-(4-F-Ph)-7-OCH_3-IQ, 1-(4-F-Ph)-6,7-$(OCH_3)_2$-IQ [36] and *cis*-$[Ru(bpy)_2Cl_2]\cdot 2H_2O$ [36] were prepared as previous literature. And these complexes were characterized by Elemental microanalyses, ESI-MS, ^{1}H NMR and UV–Vis spectra.

4.2.1. Synthesis of $[Ru(bpy)_2(1\text{-}(4\text{-}F\text{-}Ph)\text{-}IQ)](PF_6)$ (*RuIQ-3*)

A mixture of *cis*-$[Ru(bpy)_2Cl_2]\cdot 2H_2O$ (0.052 g, 0.1 mM), 1-(4-F-Ph)-IQ (0.0223 g, 0.1 mM), $Ag(CF_3SO_3)$ (0.064 g, 0.25 mM) and 10% methanol solution of $(CH_3)_4NOH$(0.012 g, 0.13 mol) in anhydrous ethanol (10 mL) was refluxed under argon at 80 °C for 12 h. After the reaction, AgCl was removed by filtration, the red precipitate (0.04 g) was then obtained by a dropwise addition of saturated aqueous KPF_6 solution. Finally, the purple-red precipitate was dried under vacuum and purified by column chromatography on neutral alumina with a mixture of CH_3CN-toluene (1:3, v/v) as eluent. Yield: 72 %. Anal. calc. for $C_{35}H_{25}F_7N_5PRu$: C, 53.83; H, 3.23; N, 8.97; found: C, 53.80; H, 3.25; N,

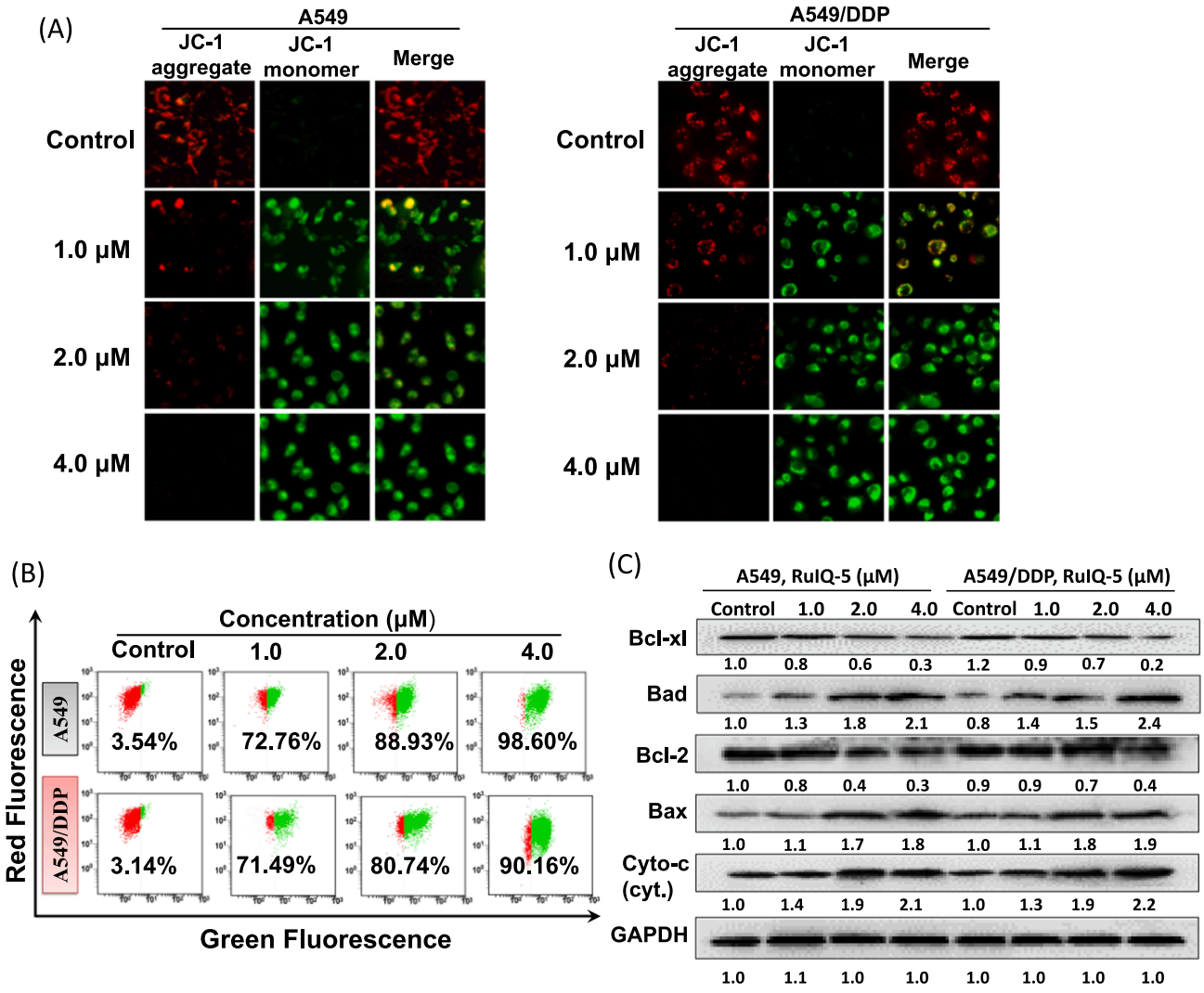

Fig. 9. RuIQ-5 induced changes of mitochondrial membrane potential (MMP) in A549 and A549/DDP cells. (A) Fluorescence microscope analysis of cellular MMP level by JC-1 staining after 1.0, 2.0 and 4.0 μM of **RuIQ-5** treatment for 24 h. (B) Flow cytometry analysis of cellular MMP level after 1.0, 2.0 and 4.0 μM of **RuIQ-5** treatment for 24 h. (C) The expression levels of Bcl-2 family proteins and cytochrome *c* in cytosol were evaluated in a concentration-dependent manner with **RuIQ-5** treatment for 24 h. GAPDH was used as internal control.

9.18. ESI-MS (MeCN): m/z = 636 ($[M - PF_6]^+$). ^{1}H NMR (400 MHz, DMSO-d_6) δ 8.93 – 8.63 (m, 5H), 8.42 (dd, J = 9.0, 5.6 Hz, 1H), 8.24 – 8.06 (m, 1H), 8.02 – 7.85 (m, 5H), 7.85 – 7.71 (m, 3H), 7.71 – 7.49 (m, 3H), 7.51 – 7.26 (m, 5H), 6.74 (td, J = 8.8, 2.8 Hz, 1H), 6.12 (dd, J = 9.2, 2.8 Hz, 1H). ^{13}C NMR (100 MHz, DMSO) δ 166.62, 163.39, 160.86, 157.56, 156.82, 156.66, 154.91, 154.13, 150.71, 149.94, 148.86, 143.61, 142.23, 137.35, 136.14, 135.93, 135.11, 134.89, 132.24, 132.15, 130.78, 129.13, 128.06, 127.52, 127.23, 127.12, 126.02, 125.98, 124.25, 124.09, 123.98, 120.67, 120.36, 120.22, 108.11, 107.89. UV–Vis (λ/nm, ε/M^{-1}•cm^{-1}) (PBS): 296 (686000), 492 (134000).

*4.2.2. Synthesis of [Ru(bpy)$_2$(1-(4-F-Ph)-7-OCH$_3$-IQ)](PF$_6$) (**RuIQ-4**)*

The synthesis route of **RuIQ-4** was similar to that of **RuIQ-3** except that the 1-(4-F-Ph)-IQ was replaced by 1-(4-F-Ph)-7-OCH$_3$-IQ. Synthesized **RuIQ-4** complex was a purple-red solid with a weigh of 0.040 g, and its yield was 60%. Anal. calc. for $C_{36}H_{27}F_7N_5OPRu$: C, 53.34; H, 3.36; N, 8.64; found: C, 53.30; H, 3.35; N, 8.63. ESI-MS (MeCN): m/z = 668.06 ($[M - PF_6]^+$). ^{1}H NMR (400 MHz, DMSO-d_6) δ 8.83 – 8.72 (m, 1H), 8.68 (dt, J = 16.2, 6.6 Hz, 3H), 8.31 (dd, J = 5.9, 1.4 Hz, 1H), 8.22 – 8.09 (m, 1H), 8.05 (ddd, J = 15.7, 7.7, 1.6 Hz, 1H), 8.01 – 7.91 (m, 4H), 7.86 – 7.71 (m, 2H), 7.65 – 7.55 (m, 1H), 7.52 – 7.43 (m, 2H), 7.43 – 7.35 (m, 3H), 7.28 (d, J = 8.4 Hz, 1H), 7.04 (dd, J = 8.3, 2.6 Hz, 1H), 6.82 – 6.65 (m, 1H), 6.66 – 6.58 (m, 1H), 6.04 (dd, J = 9.3, 2.7 Hz, 1H), 3.92 (s, 3H). ^{13}C NMR (100 MHz, DMSO) δ 164.87, 163.19, 160.66, 159.56, 157.57, 156.81, 156.67, 154.92, 154.08, 150.57, 149.92, 148.82, 143.82, 140.46, 137.30, 135.87, 135.04, 134.83, 131.54, 131.26, 131.18, 129.80, 128.01, 127.51, 127.17, 127.11, 124.24, 124.06, 123.95, 122.72, 120.45, 120.33, 120.20, 108.06, 107.84, 105.00, 55.99. UV–Vis (λ/nm, ε/M^{-1}•cm^{-1}) (PBS): 296 (36650), 492 (9300).

*4.2.3. Synthesis of [Ru(bpy)$_2$(1-(4-F-Ph)-6,7-(OCH$_3$)$_2$-IQ)](PF$_6$) (**RuIQ-5**)*

RuIQ-5 complex was synthesized in a manner identical to that described for **RuIQ-3**, except that the 1-(4-F-Ph)-IQ was replaced by 1-(4-F-Ph)-6,7-(OCH$_3$)$_2$-IQ. Synthesized **RuIQ-5** complex was a purple-red solid with a weigh of 0.042 g, and its yield was 60%. Anal. calc. for $C_{37}H_{29}F_7N_5O_2PRu$: C, 52.86; H, 3.48; N, 8.33; found: C, 52.81; H, 3.50; N, 8.30. ESI-MS (MeCN): m/z = 695.90 ($[M - PF_6]^+$). ^{1}H NMR (400 MHz, DMSO-d_6) δ 8.83 – 8.57 (m, 4H), 8.34 (dt, J = 5.6, 1.2 Hz, 1H), 8.13 – 7.87 (m, 6H), 7.87 – 7.81 (m, 1H), 7.76 – 7.69 (m, 1H), 7.60 – 7.32 (m, 7H), 6.99 (s, 1H), 6.62 (td, J = 8.9, 2.8 Hz, 1H), 6.02 (dd, J = 9.3, 2.7 Hz, 1H), 3.85 (s, 3H), 3.82 (s, 3H). ^{13}C NMR (100 MHz, DMSO) δ

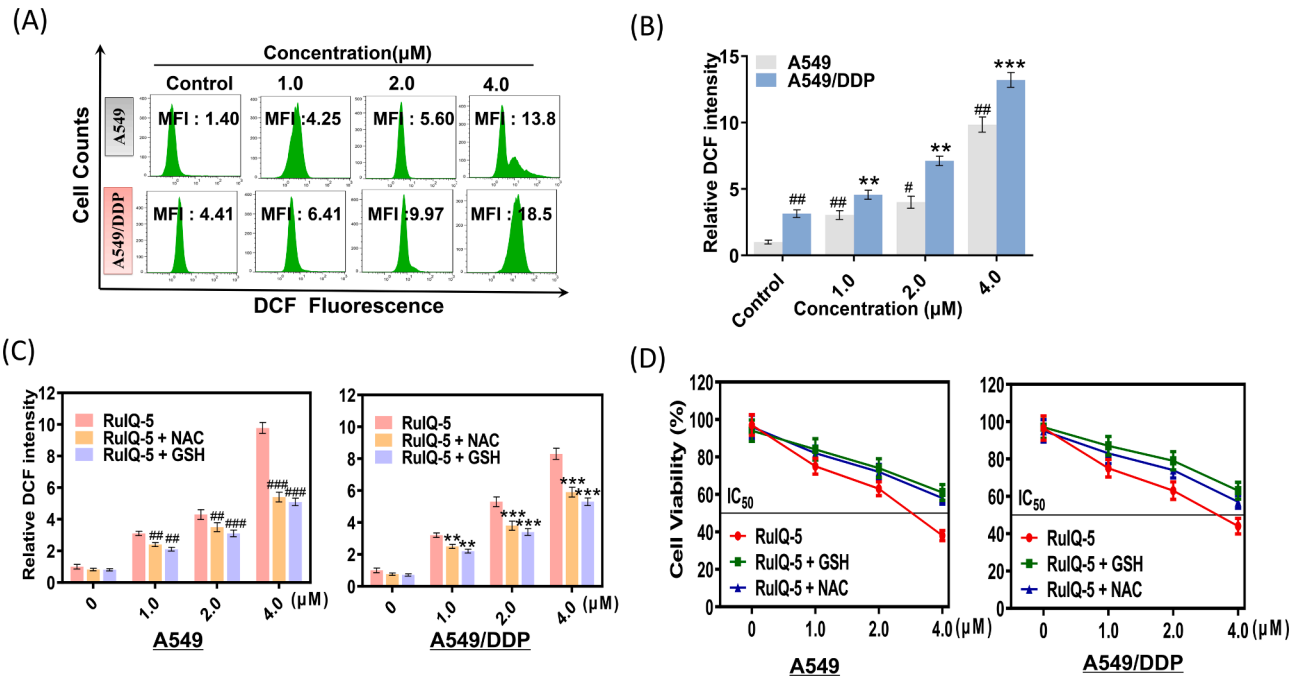

Fig. 10. Detection of ROS level after **RuIQ-5** treatment. (A) ROS generation was determined by flow cytometry, A549 and A549/DDP cells stained with DCFH-DA after **RuIQ-5** complexes treatment for 12 h. (B) Microplate analysis of cellular ROS level by DCFH-DA staining after 1.0, 2.0 and 4.0 μM of **RuIQ-5** treatment for 12 h. × ± s, n = 3. $^{\#}P < 0.05$, $^{\#\#}P < 0.01$, $^{\#\#\#}P < 0.001$ vs A549 control, $^{*}P < 0.05$, $^{**}P < 0.01$, $^{***}P < 0.001$ vs A549/DDP control. (C), (D) Effect of NAC, GSH on ROS generation and cell viability. × ± s, n = 3. $^{\#\#}P < 0.01$, $^{\#\#\#}P < 0.001$ vs A549 treatment group, $^{**}P < 0.01$, $^{***}P < 0.001$ vs A549/DDP treatment group.

163.78, 163.13, 160.61, 157.59, 156.99, 156.75, 154.98, 153.94, 152.88, 151.17, 150.46, 149.98, 148.82, 143.96, 141.02, 137.17, 135.70, 134.84, 134.66, 133.39, 130.93, 130.84, 127.95, 127.46, 127.10, 124.22, 124.03, 123.92, 121.95, 120.32, 120.18, 119.61, 107.98, 107.75, 106.63, 104.98, 56.36, 56.14. UV–Vis (λ/nm, $\varepsilon/M^{-1}\cdot cm^{-1}$) (PBS): 296 (32900), 493 (7850).

4.3. Cell lines and cell culture conditions

All human cancer cell lines studied in this work were obtained from the American Type Culture Collection (ATCC, Manassas, VA). All cell lines were maintained in DMEM culture media supplemented with 10% FBS and incubated at 37 °C in a 5% CO_2 incubator unless otherwise noted. The IC_{50} values were determined by MTT assay according to our previous report [74].

4.4. Stability assay

The stability of the Ru(II)-IQ complexes were measured by UV/Vis spectroscopy according to the methodology described in Zheng et al.' work [75]. The complexes were firstly dissolved in DMSO and then diluted with PBS. The UV/Vis spectra were recorded every 6 or 12 h for 48 h.

4.5. Viability assay (MTT assay)

The cell viability of A549, A549/DDP, HepG2, MCF-7, HBE cells after treatment with different concentrations of Ru(II)-IQ complexes **RuIQ-3**, **RuIQ-4** and **RuIQ-5** for 48 h was measured by MTT assay [74].

4.6. Antimetastatic properties

The antimetastatic property of complex **RuIQ-5** was evaluated by a wound-healing assay. A549 and A549/DDP cells were seeded in 6-well plates (each well contained 2 mL of cell culture media) and allowed to grow and form a confluent monolayer, respectively. Each well of the plates was pre-marked with a horizontal line passing through the bottom center prior to cell seeding. Wounds were created perpendicular to the lines by 10 μL tips, and detached cells were removed by washing with PBS (pH 7.4). The cells were then treated with or without 1.0, 2.0, 4.0 μM of complex **RuIQ-5** for 24 h, and the images were recorded at 0 and 24 h time point, respectively.

4.7. 3D multicellular tumor spheroids (MCTSs) formation

MCTSs were cultured using the liquid overlay method [76]. A549 or A549/DDP cells in the exponential growth phase were dissociated by a trypsin/EDTA solution to obtain single-cell suspensions. About 2500 diluted A549 or A549/DDP cells were transferred to 1% agarose-coated transparent 96-well plates with DMEM (200 mL) containing 10% FBS. A549 MCTSs and A549/DDP MCTSs formed in 4 days with diameters of approximately 400 μm at 37 °C in the presence of 5% CO_2. After the MCTS formation in 96-well plates, cells were imaged using an inverted fluorescence microscope. The diameter of each tumor spheroid was calculated by Image J software.

4.8. Cytotoxicity assay of Ru(II)-IQ complexes towards 3D MCTSs

MCTSs were generated as mentioned above. On fourth day, 50% of the plating medium were carefully replaced by fresh DMEM/FBS medium containing different concentrations of **RuIQ-5** (1.0, 2.0, 4.0 μM). In parallel, for the untreated group, 50% of the plating medium was replaced by fresh medium without **RuIQ-5**. The cytotoxicities of the ruthenium complexes were assessed for A549 and A549/DDP cells on the basis of ATP concentration using CellTiter-Lumi™ Plus luminescent cell viability assay kit (Beyotime). The fluorescence of CellTiter-Lumi™ Plus luminescent detection reagent was then measured by a microplate analyzer.

4.9. Staining of MCTSs by calcein AM/PI

The cytotoxicity of **RuIQ-5** in MCTSs was evaluated by calcein

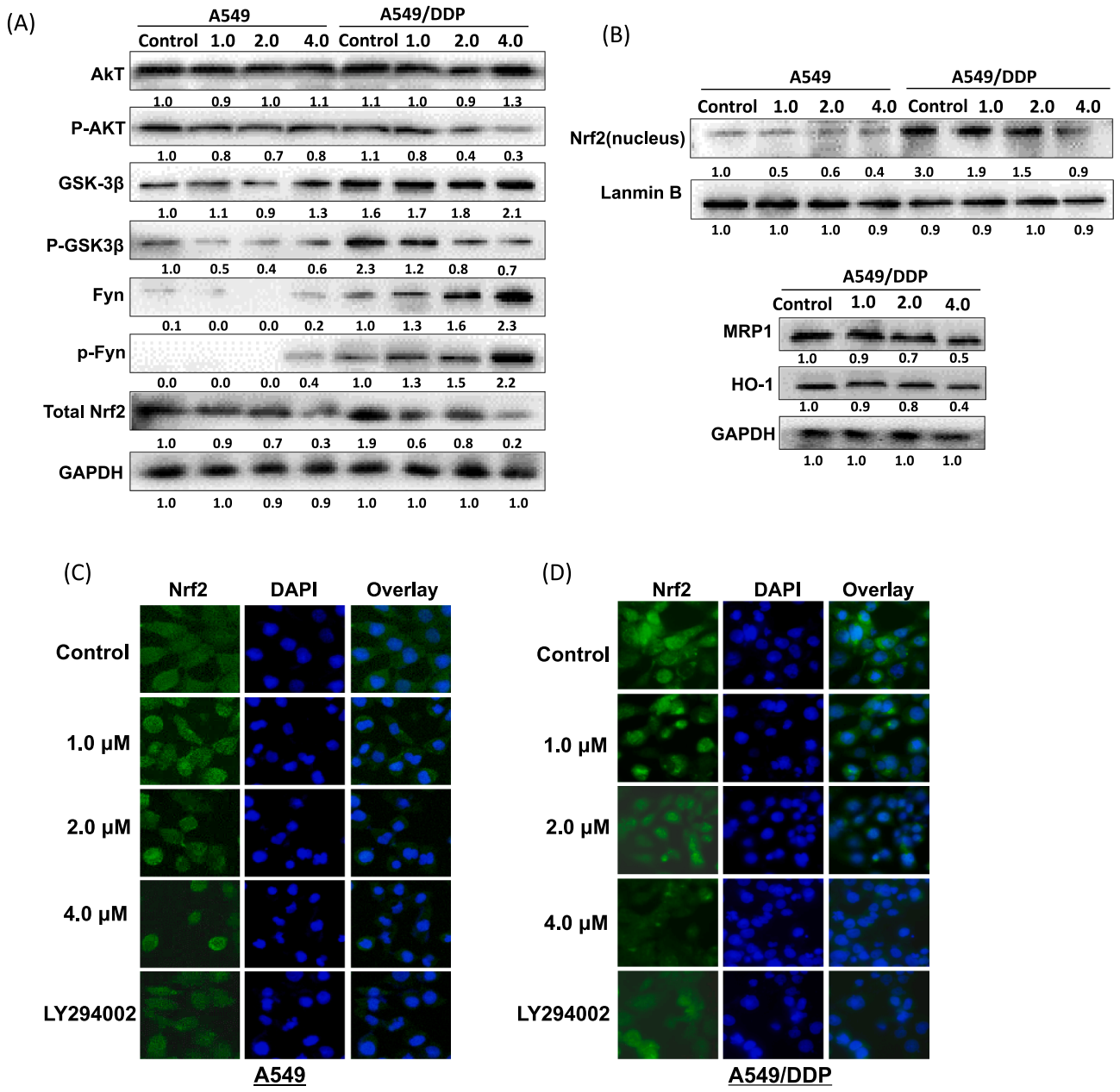

Fig. 11. Akt/GSK3β/Fyn signaling pathway involved in **RuIQ-5**-induced apoptosis. (A) Western blot analysis of Akt/GSK3β/Fyn signaling pathway related proteins in A549 and A549/DDP cells after 24 h exposure of **RuIQ-5** at indicated concentrations (1.0, 2.0, 4.0 μM). (B) Western blot analysis of nucleus Nrf2 and drug-resistance related proteins MRP1 and HO-1 in A549 and A549/DDP cells after 24 h exposure of **RuIQ-5** at indicated concentrations (1.0, 2.0, 4.0 μM). (C) and (D) Immunofluorescence staining assay of Nrf2 in A549 and A549/DDP cells after 24 h **RuIQ-5** exposures.

acetoxymethyl ester (AM) and propidium iodide (PI) double staining. Firstly, spheroids were treated with 1.0, 2.0, and 4.0 μM of **RuIQ-5** for 72 h. Treated spheroids were then stained with calcein AM (excitation at 488 nm, emission at 515 nm) and PI (excitation at 535 nm, emission at 617 nm) and subsequently imaged directly using an inverted fluorescence microscope.

4.10. Zebrafish embryotoxicity test

Zebrafish embryos were provided by the Zebrafish Platform of Affiliated hospital of Guangdong Medical University. Zebrafish embryos were incubated in 12-well plates with 2 mL of sterile dechlorinated tap water (SDTW) containing different concentrations (0, 1.7, 3.4, 6.8, 13.6, 27.2 μg/mL) of complex **RuIQ-5** at 28.0 ± 1.0 °C. Twenty zebrafish embryos were assessed in each treatment (concentration) group, respectively. Observations were recorded using a DFC310 FX microscope (Leica Microsystems CMS GmbH, Germany) every 24 h until the test ended. The ethical protocols used for the *in vivo* zebrafish embryo study were performed in compliance with the ethical regulations of Guangdong Medical University. The experiment was repeated thrice.

4.11. Measurement of lipophilicity

The distribution coefficient of each Ru(II)-IQ complex, which was presented as $\log P_{o/w}$ values, was detected by the "shake-flask" method as previously described [50]. Briefly, a suitable quantity of a stock solution of a Ru(II)-IQ complex or cisplatin in aqueous NaCl was added to an equal volume of octanol, and the mixture was shaken at 25 °C, 200 rpm for 48 h to allow partitioning, followed by centrifugation at 3000 rpm for 10 min. The resultant aqueous layer was separated from the

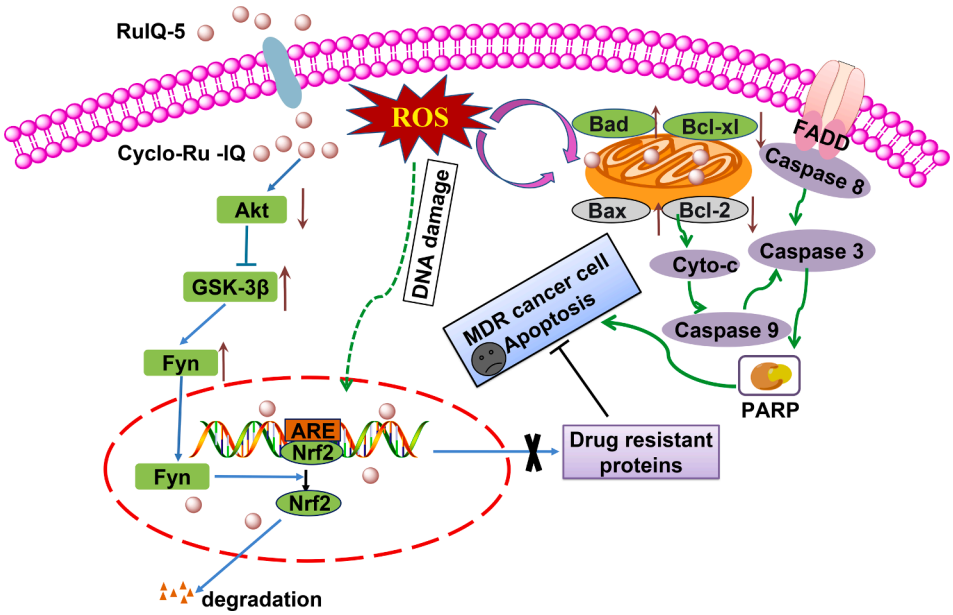

Fig. 12. Schematic illustration of the mechanism of **RuIQ-5** in reversing cisplatin resistance in A549/DDP cells.

octanol layer for Ru(II) or Pt analysis. The Ru(II) or Pt content in the aqueous layer was measured by inductively coupled plasma mass spectrometry (ICP-MS) and used to calculate the Log$P_{o/w}$ values according to the equation Log$P_{o/w}$ = Log ([Ru]$_o$/[Ru]$_w$).

4.12. Cellular uptake and localization

A549 and A549/DDP cells were cultured in 60 mm tissue culture dishes for 12 h, and then treated with 2.0 μM of **RuIQ-5** or cisplatin, respectively. Twenty-four hours after treatment, cells were collected. In order to investigate the localization of **RuIQ-5** and cisplatin in cells, different cellular fractions (nuclear, mitochondrial and cytoplasmic fractions) of A549 and A549/DDP cells were extracted using Cell Mitochondria Isolation Kit. The dishes were digested with 3 mL of concentrated nitric acid and 1 mL of perhydrol for 24 h, and then diluted to 5 mL with ultrapure water. Finally, the amount of **RuIQ-5** complexes or cisplatin uptake by A549 and A549/DDP cells was determined by ICP-MS.

4.13. Studies on the mechanism of cellular uptake

A549 and A549/DDP cells were pretreated with endocytosis inhibitors (sodium azide, NaN_3: 2.5 μM; 2-deoxy-D-glucose, 2-DOG: 10 mM; sucrose: 20 mM; and nystatin: 2.5 μg/mL) for 2 h, followed by treatment with 2 μM of **RuIQ-5** for 6 h. The cells were then trypsinized and collected, then were determined using ICP-MS.

4.14. Analysis of cell cycle arrest by flow cytometry

The cell cycle distribution was investigated by flow cytometry analysis as previously described [74,77,78]. A549 and A549/DDP cells were treated with different concentration doses (1.0, 2.0, 4.0 μM) of **RuIQ-5**, respectively. After 24 h incubation, the cells were collected and fixed in 75% ethanol at −20 °C overnight. The cell pellets were then centrifuged and washed with PBS twice, and subsequently stained with PI in the presence of RNase A (100 μM) for 30 min at 37 °C in the dark. Analysis of samples was performed using a flow cytometer.

4.15. Cell treatment with EdU

The anti-proliferation activities of **RuIQ-5** was measured using a BeyoClick EdU-594 cell proliferation assay kit (Beyotime). Firstly, A549 and A549/DDP cells were seeded into 6-well plates and then treated with different concentrations (1.0, 2.0, and 4.0 μM) of **RuIQ5** for 12 h, respectively. Then 10 μM EdU in 200 μL of DMEM/FBS medium was added to each well and the plates were incubated for 2 h. Then the cells were fixed with 4% paraformaldehyde for 15 min, washed twice with 3% bovine serum albumin (BSA), followed by cell permeabilization using 0.5% TritonX-100 for 20 min. Subsequently, the cells were washed with 3% BSA twice, and the Click-it reaction mixture was then added to each well and incubated for 30 min, followed by washing with 3% BSA. Cell nucleus staining was performed by adding Hoechst 33342 to each well and incubated for 30 min, followed by washing with PBS twice. Finally, the cells were imaged under an inverted fluorescence microscope.

4.16. Comet assay

Single-cell gel electrophoresis (SCGE), also known as comet assay, is a reliable method to detect DNA damage which is evidenced by the comet tails [74]. In this study, comet assay was performed to detect **RuIQ5**-induced DNA damage using the Comet assay reagent kit (Trevigen) according to the manufacturer's instructions. DNA of A549 and A549/DDP cells was stained with acridine orange (AO, 20 μg/mL) and then photographed by an inverted fluorescence microscope.

4.17. Apoptosis assay by AO/EB and Hoechst 33342 staining

A549 and A549/DDP cells were incubated with different concentrations (1.0, 2.0, and 4.0 μM) of **RuIQ5**, respectively. After 24 h, cell nuclei were counterstained with acridine orange/ethidium bromide (AO/EB) solution (100 μg/mL AO, 100 μg/mL EB) or Hoechst 33,342 (5 μg/mL in PBS) for 10 min followed by washing twice with PBS. Cell images were then captured by an inverted fluorescence microscope.

4.18. Apoptosis assay by annexin V/PI double staining assay

The Apoptosis assay was performed using AnnexinV-FITC Apoptosis Detection Kit as previously described [50]. A549 and A549/DDP cells were incubated with different concentrations (1.0, 2.0, and 4.0 μM) of **RuIQ5**, respectively. After 24 h, cells were harvested, washed twice with PBS, and re-suspended in 500 μL of binding buffer. The cell suspensions

were stained with 5 μL of Annexin V-FITC and 10 μL of PI at room temperature for 15 min in the dark, and subsequently analyzed using a flow cytometer.

4.19. Measurement of mitochondrial membrane potential

The mitochondrial membrane potential (MMP) was analyzed using flow cytometry and inverted fluorescence microscope as previously described [77]. The A549 or A549/DDP cells were incubated with different concentrations (1.0, 2.0, 4.0 μM) of **RuIQ-5**. After 12 h, cells were gently collected and incubated with 10 μg/mL JC-1 in 500 μL of PBS at 37 °C in the dark for 30 min. Then, the cells were re-suspended in PBS and analyzed by flow cytometer immediately. In parallel, cells collected were incubated with 10 μg/mL JC-1 in 500 μL of DMEM/FBS medium instead of PBS for 30 min, followed by washing twice with PBS and subsequently photographed using an inverted fluorescence microscope immediately.

4.20. ROS determination

ROS level was detected after staining A549 or A549/DDP cells with DCFH-DA as previously described [77]. Briefly, the A549 or A549/DDP cells were treated with different concentrations (1.0, 2.0, and 4.0 μM) of **RuIQ-5** for 12 h. Then, the cells were incubated with 10 μM DCFH-DA in fresh medium at 37 °C in the dark for 20 min. After that, cells were analyzed by flow cytometer or photographed using an inverted fluorescence microscope .

4.21. Immunofluorescence assay

Firstly, A549 or A549/DDP cells were incubated with different concentrations (1.0, 2.0, and 4.0 μM) of **RuIQ-5**. After 24 h, cells were fixed by 4% paraformaldehyde, incubated with 0.3% Triton X-100, and blocked in PBS with 30% FBS. Then, cells were sequentially incubated with anti-Nrf2 antibody (1:50 dilution) at 4℃ for 24 h, and FITC-conjugated anti-mouse IgG antibody (1:100 dilution) at room temperature for 1 h. Finally, cells were stained with 4′,6-diamidino-2-phenylindole (DAPI, 1 μg/mL) for 5 min and subsequently examined using an inverted fluorescence microscope.

4.22. Western blot assay

The effects of complex **RuIQ-5** on expression levels of Bcl-2 family proteins, caspase, and proteins related to Akt/GSK3β/Fyn signaling pathway were exanimated by western blot assay as previously described [39,74]. Proteins were visualized using ChemiDoc^{TM} XRS + Imaging System (Bio-Rad, USA).

All assays were performed at least three times, and all data were expressed as the mean ± SD.

Declaration of Competing Interest

The authors declare that they have no known competing financial interests or personal relationships that could have appeared to influence the work reported in this paper.

Acknowledgements

This research was funded by the National Natural Science Foundation of China (21701034), the Natural Science Foundation of Guangdong Province (2020A1515010444), Discipline Construction Project of Guangdong Medical University (4SG21004G), the Science and Technology Program of Guangdong Province (2019B090905011), the Fund of Southern Marine Science and Engineering Guangdong Laboratory (Zhanjiang) (ZJW-2019-007), Major Scientific Research Projects in Guangdong Province (Special Innovative Projects) (2018KQNCX100), the Medical Scientific Research Foundation of Guangdong Province of China (A2020414) and the University Student Innovation Experiment Program.

Appendix A. Supplementary material

Supplementary data to this article can be found online at https://doi.org/10.1016/j.bioorg.2021.105516.

References

[1] X.T. Hu, H.C. Song, H. Yu, Z.C. Wu, X.G. Liu, W.C. Chen, Overexpression of progerin results in impaired proliferation and invasion of non-small cell lung cancer cells, Onco. Target. Ther. 13 (2020) 2629–2642.
[2] H. Burger, W.J. Loos, K. Eechoute, J. Verweij, R.H.J. Mathijssen, E.A.C. Wiemer, Drug transporters of platinum-based anticancer agents and their clinical significance, Drug. Resist. Update. 14 (1) (2011) 22–34.
[3] L. Xiao, X. Lan, X. Shi, K. Zhao, D. Wang, X. Wang, F. Li, H. Huang, J. Liu, Cytoplasmic RAP1 mediates cisplatin resistance of non-small cell lung cancer, Cell. Death. Dis. 8 (2017) 2803–2803.
[4] G.M. DeNicola, P.H. Chen, E. Mullarky, J.A. Sudderth, Z. Hu, D. Wu, H. Tang, Y. Xie, J.M. Asara, K.E. Huffman, NRF2 regulates serine biosynthesis in non–small cell lung cancer, Nat. Genet. 47 (2015) 1475.
[5] B. Tian, Z.-N. Lu, X.-L. Guo, Regulation and role of nuclear factor-E2-related factor 2 (Nrf2) in multidrug resistance of hepatocellular carcinoma, Chem. Biol. Interact. 280 (2018) 70–76.
[6] T. Suzuki, M. Yamamoto, Molecular basis of the Keap1-Nrf2 system, Free Radic. Biol. Med. 88 (2015) 93–100.
[7] L. Ji, H. Li, P. Gao, G. Shang, D.D. Zhang, N. Zhang, T. Jiang, O. Eickelberg, Nrf2 pathway regulates multidrug-resistance-associated protein 1 in small cell lung cancer, PLoS ONE 8 (2013).
[8] A.K. Jain, A.K. Jaiswal, GSK-3beta acts upstream of Fyn kinase in regulation of nuclear export and degradation of NF-E2 related factor 2, J. Biol. Chem. 282 (2007) 16502–16510.
[9] H. Rong, Y. Liang, Y. Niu, Rosmarinic acid attenuates β-amyloid-induced oxidative stress via Akt/GSK-3β/Fyn-mediated Nrf2 activation in PC12 cells, Free Radic. Biol. Med. 120 (2018) 114–123.
[10] Y. Xin, Y. Bai, X. Jiang, S. Zhou, Y. Wang, K.A. Wintergerst, T. Cui, H. Ji, Y. Tan, L. Cai, Sulforaphane prevents angiotensin II-induced cardiomyopathy by activation of Nrf2 via stimulating the Akt/GSK-3β/Fyn pathway, Redox Biol 15 (2018) 405–417.
[11] A. Singh, S. Venkannagari, K.H. Oh, Y.-Q. Zhang, J.M. Rohde, L.i. Liu, S. Nimmagadda, K. Sudini, K.R. Brimacombe, S. Gajghate, J. Ma, A. Wang, X. Xu, S. A. Shahane, M. Xia, J. Woo, G.A. Mensah, Z. Wang, M. Ferrer, E. Gabrielson, Z. Li, F. Rastinejad, M. Shen, M.B. Boxer, S. Biswal, Small molecule inhibitor of NRF2 selectively intervenes therapeutic resistance in KEAP1-deficient NSCLC tumors, ACS Chem. Biol. 11 (11) (2016) 3214–3225.
[12] Y.H. Tong, B. Zhang, Y. Fan, N.M. Lin, Keap1-Nrf2 pathway: A promising target towards lung cancer prevention and therapeutics, Chronic Dis. Transl. Med. 1 (2015) 175–186.
[13] K.A. Kang, J.W. Hyun, Oxidative stress, Nrf2, and epigenetic modification contribute to anticancer drug resistance, Toxicol. Res. 33 (1) (2017) 1–5.
[14] J.-P. Syu, J.-T. Chi, H.-N. Kung, Nrf2 is the key to chemotherapy resistance in MCF7 breast cancer cells under hypoxia, Oncotarget 7 (12) (2016) 14659–14672.
[15] J. Zhu, H. Wang, F. Chen, H. Lv, Z. Xu, J. Fu, Y. Hou, Y. Xu, J. Pi, Triptolide enhances chemotherapeutic efficacy of antitumor drugs in non-small-cell lung cancer cells by inhibiting Nrf2-ARE activity, Toxicol. Appl. Pharmacol. 358 (2018) 1–9.
[16] Y. Zhou, Y. Zhou, K. Wang, T. Li, M. Yang, R. Wang, Y. Chen, M. Cao, R. Hu, Flumethasone enhances the efficacy of chemotherapeutic drugs in lung cancer by inhibiting Nrf2 signaling pathway, Cancer Lett. 474 (2020) 94–105.
[17] V.M. Dembitsky, T.A. Gloriozova, V.V. Poroikov, Naturally occurring plant isoquinoline N-oxide alkaloids: Their pharmacological and SAR activities, Phytomedicine 22 (2015) 183–202.
[18] Y. Song, Z. Shao, T.S. Dexheimer, E.S. Scher, Y. Pommier, M. Cushman, Structure-based design, synthesis, and biological studies of new anticancer norindenoisoquinoline topoisomerase I inhibitors, J. Med. Chem. 53 (5) (2010) 1979–1989.
[19] Y. Feng, Y. Hu, J. Cen, K.N. Darshika, W. Fang, Y. Li, W. Huang, HZ08 inhibits the multi-drug resistance on multiple sites as the substrate of p-glycoprotein, Eur. J. Pharmacol. 712 (1-3) (2013) 53–59.
[20] F. Zhang, X. Wang, X. Xu, M. Li, J. Zhou, W. Wang, Reconstituted high density lipoprotein mediated targeted co-delivery of HZ08 and paclitaxel enhances the efficacy of paclitaxel in multidrug-resistant MCF-7 breast cancer cells, Eur. J. Pharm. Sci. 92 (2016) 11–21.
[21] Y.u. Lei, J. Tan, M. Wink, Y. Ma, N.a. Li, G. Su, An isoquinoline alkaloid from the Chinese herbal plant Corydalis yanhusuo WT Wang inhibits P-glycoprotein and multidrug resistance-associate protein 1, Food Chem. 136 (3-4) (2013) 1117–1121.
[22] Z.-X. Qing, J.-L. Huang, X.-Y. Yang, J.-H. Liu, H.-L. Cao, F. Xiang, P.i. Cheng, J.-G. Zeng, Anticancer and Reversing Multidrug Resistance Activities of Natural Isoquinoline Alkaloids and their Structure-activity Relationship, Curr. Med. Chem. 25 (38) (2019) 5088–5114.

[23] K.B. Huang, H.Y. Mo, Z.F. Chen, J.H. Wei, Y.C. Liu, H. Liang, Isoquinoline derivatives Zn(II)/Ni(II) complexes: Crystal structures, cytotoxicity, and their action mechanism, Eur. J. Med. Chem. 100 (2015) 68–76.

[24] J.-C. Chen, Y. Zhang, X.-M. Jie, J.i. She, G.-Z. Dongye, Y.u. Zhong, Y.-Y. Deng, J. Wang, B.-Y. Guo, L.-M. Chen, Ruthenium (II) salicylate complexes inducing ROS-mediated apoptosis by targeting thioredoxin reductase, J. Inorg. Biochem. 193 (2019) 112–123.

[25] S. Thota, D.A. Rodrigues, D.C. Crans, E.J. Barreiro, Ru(II) Compounds: Next-Generation Anticancer Metallotherapeutics? J. Med. Chem. 61 (2018) 5805–5821.

[26] A. Bergamo, L. Messori, F. Piccioli, M. Cocchietto, G. Sava, Biological role of adduct formation of the ruthenium (III) complex NAMI-A with serum albumin and serum transferrin, Invest. New Drugs 21 (2003) 401–411.

[27] E. Alessio, G. Mestroni, A. Bergamo, G. Sava, Ruthenium antimetastatic agents, Curr. Top. Med. Chem. 4 (2004) 1525–1535.

[28] C. Hartinger, M. Jakupec, S. Zorbas-Seifried, M. Groessl, A. Egger, W. Berger, H. Zorbas, P. Dyson, B. Keppler, KP1019, a new redox-active anticancer agent–Preclinical development and results of a clinical phase I study in tumor patients, Chem. Biodivers. 5 (10) (2008) 2140–2155.

[29] C.G. Hartinger, S. Zorbas-Seifried, M.A. Jakupec, B. Kynast, H. Zorbas, B. K. Keppler, From bench to bedside–preclinical and early clinical development of the anticancer agent indazolium trans-[tetrachlorobis (1H-indazole) ruthenate (III)](KP1019 or FFC14A), J. Inorg. Biochem. 100 (5-6) (2006) 891–904.

[30] L. Zeng, P. Gupta, Y. Chen, E. Wang, L. Ji, H. Chao, Z.-S. Chen, The development of anticancer ruthenium (II) complexes: from single molecule compounds to nanomaterials, Chem. Soc. Rev. 46 (2017) 5771–5804.

[31] D.A. Smithen, H. Yin, M.H.R. Beh, M. Hetu, T.S. Cameron, S.A. McFarland, A. Thompson, Synthesis and photobiological activity of Ru (II) dyads derived from pyrrole-2-carboxylate thionoesters, Inorg. Chem. 56 (7) (2017) 4121–4132.

[32] J.É. Debreczeni, A.N. Bullock, G.E. Atilla, D.S. Williams, H. Bregman, S. Knapp, E. Meggers, Ruthenium half-sandwich complexes bound to protein kinase Pim-1, Angew. Chem. Int. Ed. 45 (10) (2006) 1580–1585.

[33] L. Zeng, Y.u. Chen, H. Huang, J. Wang, D. Zhao, L. Ji, H. Chao, Cyclometalated ruthenium (II) anthraquinone complexes exhibit strong anticancer activity in hypoxic tumor cells, Chem.–A Eur. J. 21 (43) (2015) 15308–15319.

[34] L. Zeng, Y. Chen, J. Liu, H. Huang, R. Guan, L. Ji, H. Chao, Ruthenium (II) complexes with 2-phenylimidazo [4, 5-f][1, 10] phenanthroline derivatives that strongly combat cisplatin-resistant tumor cells, Sci. Rep. 6 (2016) 1–13.

[35] H. Huang, P. Zhang, Y. Chen, K. Qiu, C. Jin, L. Ji, H. Chao, Synthesis, characterization and biological evaluation of labile intercalative ruthenium (II) complexes for anticancer drug screening, Dalton Trans. 45 (2016) 13135–13145.

[36] J. Dong, X.-X. Shi, J.-J. Yan, J. Xing, Q. Zhang, S. Xiao, Efficient and Practical One-Pot Conversions of N-Tosyltetrahydroisoquinolines into Isoquinolines and of N-Tosyltetrahydro-β-carbolines into β-Carbolines through Tandem β-Elimination and Aromatization, Eur. J. Org. Chem. 2010 (36) (2010) 6987–6992.

[37] B.P. Sullivan, D.J. Salmon, T.J. Meyer, Mixed Phosphine 2,2'-Bipyridine Complexes of Ruthenium, Inorg. Chem. 17 (12) (1978) 3334–3341.

[38] J.P. Collin, J.P. Sauvage, Synthesis and study of mononuclear ruthenium(II) complexes of sterically hindering diimine chelates. Implications for the catalytic oxidation of water to molecular oxygen, Inorg. Chem. 25 (2) (1986) 135–141.

[39] J. Chen, J. Wang, Y. Deng, B. Li, C. Li, Y. Lin, D. Yang, H. Zhang, L. Chen, T. Wang, Novel cyclometalated Ru(II) complexes containing isoquinoline ligands: Synthesis, characterization, cellular uptake and in vitro cytotoxicity, Eur. J. Med. Chem. 203 (2020), 112562.

[40] H. Huang, P. Zhang, H. Chen, L. Ji, H. Chao, Comparison Between Polypyridyl and Cyclometalated Ruthenium(II) Complexes: Anticancer Activities Against 2D and 3D Cancer Models, Chem. – A Eur. J. 21 (2015) 715–725.

[41] L. Ma, R. Ma, Z. Wang, S.-M. Yiu, G. Zhu, Heterodinuclear Pt (iv)–Ru (ii) anticancer prodrugs to combat both drug resistance and tumor metastasis, Chem. Commun. 52 (2016) 10735–10738.

[42] J. Friedrich, C. Seidel, R. Ebner, L.A. Kunz-Schughart, Spheroid-based drug screen: considerations and practical approach, Nat. Protoc. 4 (2009) 309.

[43] N. Yamamoto, A.K. Renfrew, B.J. Kim, N.S. Bryce, T.W. Hambley, Dual targeting of hypoxic and acidic tumor environments with a cobalt (III) chaperone complex, J. Med. Chem. 55 (24) (2012) 11013–11021.

[44] J.Z. Zhang, N.S. Bryce, A. Lanzirotti, C.K. Chen, D. Paterson, M.D. de Jonge, D. L. Howard, T.W. Hambley, Getting to the core of platinum drug bio-distributions: the penetration of anti-cancer platinum complexes into spheroid tumour models, Metallomics 4 (2012) 1209–1217.

[45] O.A. Lenis Rojas, C. Roma Rodrigues, A.R. Fernandes, F. Marques, D. Pérez Fernández, J. Guerra Varela, L. Sánchez, D. Vázquez García, M. López Torres, A. Fernández, J.J. Fernández, Dinuclear $Ru^{II}(bipy)_2$ Derivatives: Structural, Biological, and in Vivo Zebrafish Toxicity Evaluation, Inorg. Chem. 56 (2017) 7127–7144.

[46] O.A. Lenis-Rojas, M.P. Robalo, A.I. Tomaz, A. Carvalho, A.R. Fernandes, F. Marques, M. Folgueira, J. Yáñez, D. Vázquez-García, M. López Torres, A. Fernández, J.J. Fernández, Ru(II)(p-cymene) Compounds as Effective and Selective Anticancer Candidates with No Toxicity in Vivo, Inorg. Chem. 57 (21) (2018) 13150–13166.

[47] M. Bai, T. Pan, G. Yu, Q. Xie, Z. Zeng, Y. Zhang, D. Zhu, L. Mu, J. Qian, B. Chang, W.J. Mei, S. Guan, Chiral ruthenium(II) complex Delta-[$Ru(bpy)_2$(o-FMPIP)] (bpy = bipyridine, o-FMPIP = 2-(2'-trifluoromethyphenyl) imidazo[4,5-f][1,10] phenanthroline) as potential apoptosis inducer via DNA damage, Eur. J. Pharmacol. 853 (2019) 49–55.

[48] L. Zeng, Y. Chen, J. Liu, H. Huang, R. Guan, L. Ji, H. Chao, Ruthenium(II) Complexes with 2-Phenylimidazo[4,5-f][1,10]phenanthroline Derivatives that Strongly Combat Cisplatin-Resistant Tumor Cells, Sci. Rep. 6 (1) (2016) 19449.

[49] H. Huang, P. Zhang, B. Yu, Y.u. Chen, J. Wang, L. Ji, H. Chao, Targeting nucleus DNA with a Cyclometalated Dipyridophenazineruthenium(II) Complex, J. Med. Chem. 57 (21) (2014) 8971–8983.

[50] J. Chen, F.a. Peng, Y. Zhang, B. Li, J.i. She, X. Jie, Z. Zou, M. Chen, L. Chen, Synthesis, characterization, cellular uptake and apoptosis-inducing properties of two highly cytotoxic cyclometalated ruthenium(II) β-carboline complexes, Eur. J. Med. Chem. 140 (2017) 104–117.

[51] J. Chen, Y. Zhang, G. Li, F.a. Peng, X. Jie, J.i. She, G. Dongye, Z. Zou, S. Rong, L. Chen, Cytotoxicity in vitro, cellular uptake, localization and apoptotic mechanism studies induced by ruthenium(II) complex, J. Biol. Inorg. Chem. 23 (2) (2018) 261–275.

[52] W. Cao, W. Zheng, T. Chen, Ruthenium polypyridyl complex inhibits growth and metastasis of breast cancer cells by suppressing FAK signaling with enhancement of TRAIL-induced apoptosis, Sci. Rep. 5 (2015) 9157.

[53] Q. He, L. Man, Y. Ji, F. Ding, Comparison in the biological characteristics between primary cultured sensory and motor Schwann cells, Neurosci. Lett. 521 (1) (2012) 57–61.

[54] C. Alapetite, T. Wachter, E. Sage, E. Moustacchi, Use of the alkaline comet assay to detect DNA repair deficiencies in human fibroblasts exposed to UVC, UVB, UVA and gamma-rays, Int. J. Radiat Biol. 69 (1996) 359–369.

[55] W.P. Roos, B. Kaina, DNA damage-induced cell death by apoptosis, Trends Mol. Med. 12 (9) (2006) 440–450.

[56] S.-H. Lai, G.-B. Jiang, J.-H. Yao, W. Li, B.-J. Han, C. Zhang, C.-C. Zeng, Y.-J. Liu, Cytotoxic activity, DNA damage, cellular uptake, apoptosis and western blot analysis of ruthenium(II) polypyridyl complex against human lung decarcinoma A549 cell, J. Inorg. Biochem. 152 (2015) 1–9.

[57] P. Duez, G. Dehon, A. Kumps, J. Dubois, Statistics of the Comet assay: a key to discriminate between genotoxic effects, Mutagenesis 18 (2003) 159–166.

[58] Z. Tian, J. Li, S. Zhang, Z. Xu, Y. Yang, D. Kong, H. Zhang, X. Ge, J. Zhang, Z. Liu, Lysosome-targeted chemotherapeutics: half-sandwich ruthenium (II) complexes that are selectively toxic to cancer cells, Inorg. Chem. 57 (2018) 10498–10502.

[59] H. Chen, P. Wang, Z. Du, G. Wang, S. Gao, Oxidative stress, cell cycle arrest, DNA damage and apoptosis in adult zebrafish (Danio rerio) induced by tris (1, 3-dichloro-2-propyl) phosphate, Aquat. Toxicol. 194 (2018) 37–45.

[60] C. Zhang, C.-C. Zeng, S.-H. Lai, D.-G. Xing, W. Li, B.-J. Han, Y.-J. Liu, Synthesis, cytotoxicity in vitro, apoptosis, cell cycle arrest and comet assay of asymmetry ruthenium (II) complexes, Polyhedron 106 (2016) 115–124.

[61] T. Yagami, Y. Yamamoto, H. Koma, The role of secretory phospholipase A 2 in the central nervous system and neurological diseases, Mol. Neurobiol. 49 (2) (2014) 863–876.

[62] H. Lai, Z. Zhao, L. Li, W. Zheng, T. Chen, Antiangiogenic ruthenium (II) benzimidazole complexes, structure-based activation of distinct signaling pathways, Metallomics 7 (2015) 439–447.

[63] V. Venkatesh, R. Berrocal-Martin, C.J. Wedge, I. Romero-Canelón, C. Sanchez-Cano, J.-I. Song, J.P.C. Coverdale, P. Zhang, G.J. Clarkson, A. Habtemariam, S. W. Magennis, R.J. Deeth, P.J. Sadler, Mitochondria-targeted spin-labelled luminescent iridium anticancer complexes, Chem. Sci. 8 (12) (2017) 8271–8278.

[64] I.M. Ghobrial, T.E. Witzig, A.A. Adjei, Targeting apoptosis pathways in cancer therapy, CA Cancer J. Clin. 55 (3) (2005) 178–194.

[65] T. Chen, Y. Wong, Selenocystine induces apoptosis of A375 human melanoma cells by activating ROS-mediated mitochondrial pathway and p53 phosphorylation, Cell. Mol. Life Sci. 65 (2008) 2763.

[66] Z. Zhang, Q. Wu, X.-H. Wu, F.-Y. Sun, L.-M. Chen, J.-C. Chen, S.-L. Yang, W.-J. Mei, Ruthenium(II) complexes as apoptosis inducers by stabilizing c-myc G-quadruplex DNA, Eur. J. Med. Chem. 80 (2014) 316–324.

[67] T. Chen, Y.-S. Wong, Selenocystine induces caspase-independent apoptosis in MCF-7 human breast carcinoma cells with involvement of p53 phosphorylation and reactive oxygen species generation, Int. J. Biochem. Cell Biol. 41 (3) (2009) 666–676.

[68] J.-H. Lee, Y.-S. Won, K.-H. Park, M.-K. Lee, H. Tachibana, K. Yamada, K.-I. Seo, Celastrol inhibits growth and induces apoptotic cell death in melanoma cells via the activation ROS-dependent mitochondrial pathway and the suppression of PI3K/AKT signaling, Apoptosis 17 (12) (2012) 1275–1286.

[69] R.W. Robey, K.M. Pluchino, M.D. Hall, A.T. Fojo, S.E. Bates, M.M. Gottesman, Revisiting the role of ABC transporters in multidrug-resistant cancer, Nat. Rev. Cancer 18 (7) (2018) 452–464.

[70] Q. Cui, J.-Q. Wang, Y.G. Assaraf, L. Ren, P. Gupta, L. Wei, C.R. Ashby, D.-H. Yang, Z.-S. Chen, Modulating ROS to overcome multidrug resistance in cancer, Drug Resist. Updat. 41 (2018) 1–25.

[71] S. Homma, Y. Ishii, Y. Morishima, T. Yamadori, Y. Matsuno, N. Haraguchi, N. Kikuchi, H. Satoh, T. Sakamoto, N. Hizawa, K. Itoh, M. Yamamoto, Nrf2 enhances cell proliferation and resistance to anticancer drugs in human lung cancer, Clin. Cancer Res. 15 (10) (2009) 3423–3432.

[72] Y. Tian, Q. Liu, X. He, X. Yuan, Y. Chen, Q. Chu, K. Wu, Emerging roles of Nrf2 signal in non-small cell lung cancer, J. Hematol. Oncol. 9 (2016) 14.

[73] S. Chowdhry, Y. Zhang, M. McMahon, C. Sutherland, A. Cuadrado, J.D. Hayes, Nrf2 is controlled by two distinct β-TrCP recognition motifs in its Neh6 domain, one of which can be modulated by GSK-3 activity, Oncogene 32 (32) (2013) 3765–3781.

[74] L.-M. Chen, F.a. Peng, G.-D. Li, X.-M. Jie, K.-R. Cai, C. Cai, Y.u. Zhong, H. Zeng, W. u. Li, Z. Zhang, J.-C. Chen, The studies on the cytotoxicity in vitro, cellular uptake, cell cycle arrest and apoptosis-inducing properties of ruthenium methylimidazole complex $[Ru(MeIm)_4(p\text{-}cpip)]^{2+}$, J. Inorg. Biochem. 156 (2016) 64–74.

[75] Y. Zheng, L. He, D.Y. Zhang, C.P. Tan, L.N. Ji, Z.W. Mao, Mixed-ligand iridium(iii) complexes as photodynamic anticancer agents, Dalton Trans. 46 (2017) 11395–11407.

[76] G.Y. Lee, P.A. Kenny, E.H. Lee, M.J. Bissell, Three-dimensional culture models of normal and malignant breast epithelial cells, Nat. Methods 4 (4) (2007) 359–365.
[77] J.-C. Chen, G.-D. Li, F.a. Peng, X.-M. Jie, G.-Z. Dongye, Y.u. Zhong, R.-B. Feng, B.-J. Li, J.-Y. Qu, Y. Ding, L.-M. Chen, Investigation of inducing apoptosis in human lung cancer A549 cells and related mechanism of a ruthenium (II) polypyridyl complex, Inorg. Chem. Commun. 69 (2016) 35–39.
[78] L. Chen, G. Li, F.a. Peng, X. Jie, G. Dongye, K. Cai, R. Feng, B. Li, Q. Zeng, K. Lun, J. Chen, B. Xu, The induction of autophagy against mitochondria-mediated apoptosis in lung cancer cells by a ruthenium (II) imidazole complex, Oncotarget 7 (49) (2016) 80716–80734.